

SOURCE
DATATRANSPARENT
PROCESSOPEN
ACCESS

Combinatorial activation of the WNT-dependent fibrogenic program by distinct complement subunits in dystrophic muscle

Francesca Florio^{1,2,3} , Sara Vencato^{1,2}, Filomena T Papa^{1,2} , Michela Libergoli^{1,2} , Eyemen Kheir^{1,2} , Imen Ghzaïel^{1,2} , Thomas A Rando⁴, Yvan Torrente^{3,5} & Stefano Biressi^{1,2,*}

Abstract

Fibrosis is associated with compromised muscle functionality in Duchenne muscular dystrophy (DMD). We report observations with tissues from dystrophic patients and mice supporting a model to explain fibrosis in DMD, which relies on the crosstalk between the complement and the WNT signaling pathways and the functional interactions of two cellular types. Fibro-adipogenic progenitors and macrophages, which populate the inflamed dystrophic muscles, act as a combinatorial source of WNT activity by secreting distinct subunits of the C1 complement complex. The resulting aberrant activation of the WNT signaling in responsive cells, such as fibro-adipogenic progenitors, contributes to fibrosis. Indeed, pharmacological inhibition of the C1r/s subunits in a murine model of DMD mitigated the activation of the WNT signaling pathway, reduced the fibrogenic characteristics of the fibro-adipogenic progenitors, and ameliorated the dystrophic phenotype. These studies shed new light on the molecular and cellular mechanisms responsible for fibrosis in muscular dystrophy and open to new therapeutic strategies.

Keywords complement C1 complex; Duchenne muscular dystrophy; fibro-adipogenic progenitors; fibrosis; skeletal muscle regeneration

Subject Category Musculoskeletal System

DOI 10.15252/emmm.202317405 | Received 10 January 2023 |

Revised 10 October 2023 | Accepted 11 October 2023 | Published online 6 November 2023

EMBO Mol Med (2023) 15: e17405

Introduction

Duchenne muscular dystrophy (DMD) is one of the most severe and frequent forms of dystrophy (Emery, 2002; Mercuri *et al.*, 2019). DMD patients show progressive dysfunction of skeletal and cardiac muscles (Emery, 2002; Mercuri *et al.*, 2019). Although

multidisciplinary care and glucocorticoid treatment are associated with reduced disease progression and improved patient survival, no definitive cure is currently available for DMD, and patients die by their third decade of life (Birnkranz *et al.*, 2018; McDonald *et al.*, 2018). DMD occurs due to mutations in the X-chromosome dystrophin gene (O'Brien & Kunkel, 2001). The absence of functional dystrophin causes repetitive cycles of degeneration/regeneration of the muscle fibers. Portions of the dystrophic muscles (regeneration foci) continuously attempt to regenerate and are characterized by the infiltration of inflammatory cells (Ciciliot & Schiaffino, 2010). This chronic condition of inflammation and degeneration determines impairment of muscle repair potential, and fibrotic extracellular matrix progressively substitutes contractile fibers, determining a severe deficit of muscular function (Ciciliot & Schiaffino, 2010).

Upon damage, muscle regeneration is ensured by muscle satellite cells (MuSCs), a muscle-specific stem cell population required to restore tissue functionality (Scharner & Zammit, 2011). MuSCs' activity is influenced by intrinsic and extrinsic factors (Sousa-Victor *et al.*, 2022). Particularly, MuSCs function is supported by a heterogeneous pool of cells occupying the interstitial space between fibers or associated with the vasculature (Wosczyzna & Rando, 2018). Among them, mesenchymal cells, called fibro-adipogenic progenitors (FAPs), characterized by the expression of PDGF receptor- α (PDGFR α) and Sca1 critically influence muscle regeneration and homeostasis (Joe *et al.*, 2010; Uezumi *et al.*, 2010; Wosczyzna *et al.*, 2019). Moreover, a large body of evidence identified various subpopulations of immune cells as crucial mediators of effective muscle repair (Shen *et al.*, 2008; Burzyn *et al.*, 2013; Heredia *et al.*, 2013; Lemos *et al.*, 2015; Liu *et al.*, 2017). Importantly, in diseased muscle, macrophages' fate is disturbed, and the communication between MuSCs and different subpopulations of inflammatory and interstitial cells is compromised (Tidball & Villalta, 2010; Mozzetta *et al.*, 2013). These alterations are believed to contribute to the defective regeneration and promotion of fibrosis (Desguerre *et al.*, 2009; Serrano & Munoz-Canoves, 2010).

1 Department of Cellular, Computational and Integrative Biology (CIBIO), University of Trento, Trento, Italy

2 Dulbecco Telethon Institute at University of Trento, Trento, Italy

3 Neurology Unit, Fondazione IRCCS Ca' Granda Ospedale Maggiore Policlinico, Milan, Italy

4 Broad Stem Cell Research Center, University of California Los Angeles, Los Angeles, CA, USA

5 Stem Cell Laboratory, Dino Ferrari Center, Department of Pathophysiology and Transplantation, University of Milan, Milan, Italy

*Corresponding author. Tel: ++39 0461285290; E-mail: stefano.biressi@unitn.it

Multiple cell types aberrantly secrete extracellular matrix in the dystrophic setting, particularly collagens 1 and 3, which predominate in fibrotic DMD muscle (Foidart *et al*, 1981). MuSCs and cells belonging to the endothelial and hematopoietic lineage adopt fibrogenic features in DMD (Biressi *et al*, 2014; Pessina *et al*, 2015; Wang *et al*, 2016; Florio *et al*, 2022). Nevertheless, an increasing amount of evidence proposes FAPs as a major cellular source for fibrotic tissue in dystrophic muscle (Molina *et al*, 2021). A subset of PDGFR α ^{+ve} stromal cells activated upon acute injury in the muscle reportedly gives rise to a significant fraction of collagen-1-overproducing cells generated during transient scarring, typical of the healing process (Dulauroy *et al*, 2012). Genetic ablation of this fraction is sufficient to limit interstitial collagen accumulation (Dulauroy *et al*, 2012). The accumulation of PDGFR α ^{+ve} cells expressing fibrosis markers (i.e., Col1a1, Col3a1, and CTGF) in the diaphragm in the MDX dystrophic murine model supports the involvement of FAPs in the process of fibrosis not only during an acute injury but also in DMD (Uezumi *et al*, 2011). In keeping with this, interfering *in vivo* with the profibrotic PDGF-signaling pathway alters FAPs activation and fibrosis (Ieronimakis *et al*, 2016; Mueller *et al*, 2016).

The canonical WNT signaling is progressively acquiring a central role in different tissues, including skeletal muscle (Cisternas *et al*, 2014). Increased canonical WNT signaling has been reported in muscles of the MDX mice and DMD patients (Trensz *et al*, 2010; Biressi *et al*, 2014; Liu *et al*, 2016). In MDX muscle, WNT signaling promotes collagen deposition by increasing the proliferation of resident Sca1^{+ve} cells (Trensz *et al*, 2010). This observation finds parallelism in the aging muscle, also characterized by WNT-dependent defective regeneration and fibrosis (Brack *et al*, 2007; Naito *et al*, 2012). In both aging and dystrophic muscles, the activation of the canonical WNT signaling is associated with the acquisition of fibrotic features by MuSCs (Brack *et al*, 2007; Biressi *et al*, 2014). Particularly, MuSCs' loss of myogenic properties in dystrophic muscles depends on the presence of TGF β , as the administration of a TGF β -blocking antibody was able to normalize the expression of myogenic and fibrotic markers (Biressi *et al*, 2014). The profibrotic role of WNT signaling is further corroborated by its ability to establish a reciprocal reinforcing crosstalk with the TGF β -signaling pathway, which is a powerful promoter of fibrosis (Girardi & Le Grand, 2018). On the one hand, the canonical WNT signaling was shown to promote the expression of TGF β , particularly the TGF β 2 isoform (Carthy *et al*, 2011; Biressi *et al*, 2014). On the other hand, TGF β facilitates the activation of the WNT signaling pathway by different mechanisms, which include the modulation of the secretion of the WNT antagonist Dickkopf-1 and various WNT proteins or the involvement of microRNAs capable of targeting multiple components of the WNT/TGF β axis (Akhmetshina *et al*, 2012; Blyszczuk *et al*, 2017; Seo *et al*, 2018).

DMD is characterized by chronic inflammation, and the involvement of cells and signaling cascades that are part of the innate immune system is just beginning to be investigated in dystrophic tissues (Porter *et al*, 2002; Tidball & Villalta, 2010; Tripodi *et al*, 2021). The role played by the complement cascade in this context is poorly understood (Engel & Biesecker, 1982; Sewry *et al*, 1987; Spuler & Engel, 1998). Intriguingly, recent reports indicate that in addition to its role as initiator of the classical complement cascade, the complement complex C1 is able to directly activate the canonical WNT

signaling pathway (Naito *et al*, 2012; Sumida *et al*, 2015). This activation requires the presence of the C1q component of the complex (formed by C1qa, b, and c subunits codified by three genes aligned on the same chromosome) that binds to the frizzled WNT receptor and exposes the WNT co-receptor LRP6 to the enzymatic activity of the two other subunits of the C1 complex, the C1r and C1s esterases (also codified by adjacent genes) (Kusumoto *et al*, 1988; Sellar *et al*, 1991; Naito *et al*, 2012). The result of this interaction is the cleavage of the extracellular domain of the WNT co-receptor LRP that determines the activation of the WNT signaling pathway (Naito *et al*, 2012). Although several orders of magnitude weaker compared to the activation induced by the binding of the canonical WNT ligands to the Frizzled receptors, the activation of the WNT signaling pathway by the C1 complex is reportedly sufficient to promote defective regeneration and fibrosis in aging muscle (Naito *et al*, 2012). Given the even greater inflammation and disruption of regenerative potential in dystrophic muscle, we hypothesized the involvement of the complement C1/WNT axis in the progression of DMD.

We present data suggesting a causal link between the upregulation of complement C1 and the accumulation of fibrotic tissue typical of the dystrophic setting. Performing a molecular investigation in tissues from DMD patients and dystrophic animal models, we propose that distinct cell types (i.e., macrophages and FAPs) colonizing the inflamed dystrophic muscles can act as a combinatorial source of WNT activity by secreting distinct subunits of the C1 complement complex. The resulting aberrant activation of the complement C1/WNT axis in dystrophic muscles induces a cascade of events promoting fibrosis. Using an *in vivo* pharmacological approach in an accelerated murine model of DMD, we observed that halting the enzymatic activity of C1r/s normalizes the expression of fibrotic genes in FAPs and improves the muscle condition.

Results

Complement C1 is locally produced in dystrophic muscles

Different research groups, including ours, have shown enhanced canonical WNT signaling pathway activity in both dystrophic and aged mice (Appendix Fig S1A) (Brack *et al*, 2007; Trensz *et al*, 2010; Naito *et al*, 2012; Biressi *et al*, 2014). An increment in canonical WNT signaling also characterizes the muscles of DMD patients, as disclosed by the quantification of known targets of the WNT signaling pathway (i.e., Axin2 and TGF β 2) in the interstitial space of human muscle biopsies (Appendix Fig S1B and C). Among the various cell types colonizing the muscle interstitium, FAPs are characterized by an active WNT signaling pathway in the MDX dystrophic environment, which parallels a robust transcription of fibrogenic markers, including collagens 1 and 3 (Figs 1A–F and EV1A–H).

Increased levels of complement proteins in the serum have been reported to lead to increased activity of the WNT signaling pathway in old mice (Naito *et al*, 2012). To evaluate whether the factors that contribute to the enhanced WNT signaling in the dystrophic muscle have a serum origin, C2C12 myoblasts were cultured in the presence of serum collected from MDX and WT mice of different ages. The

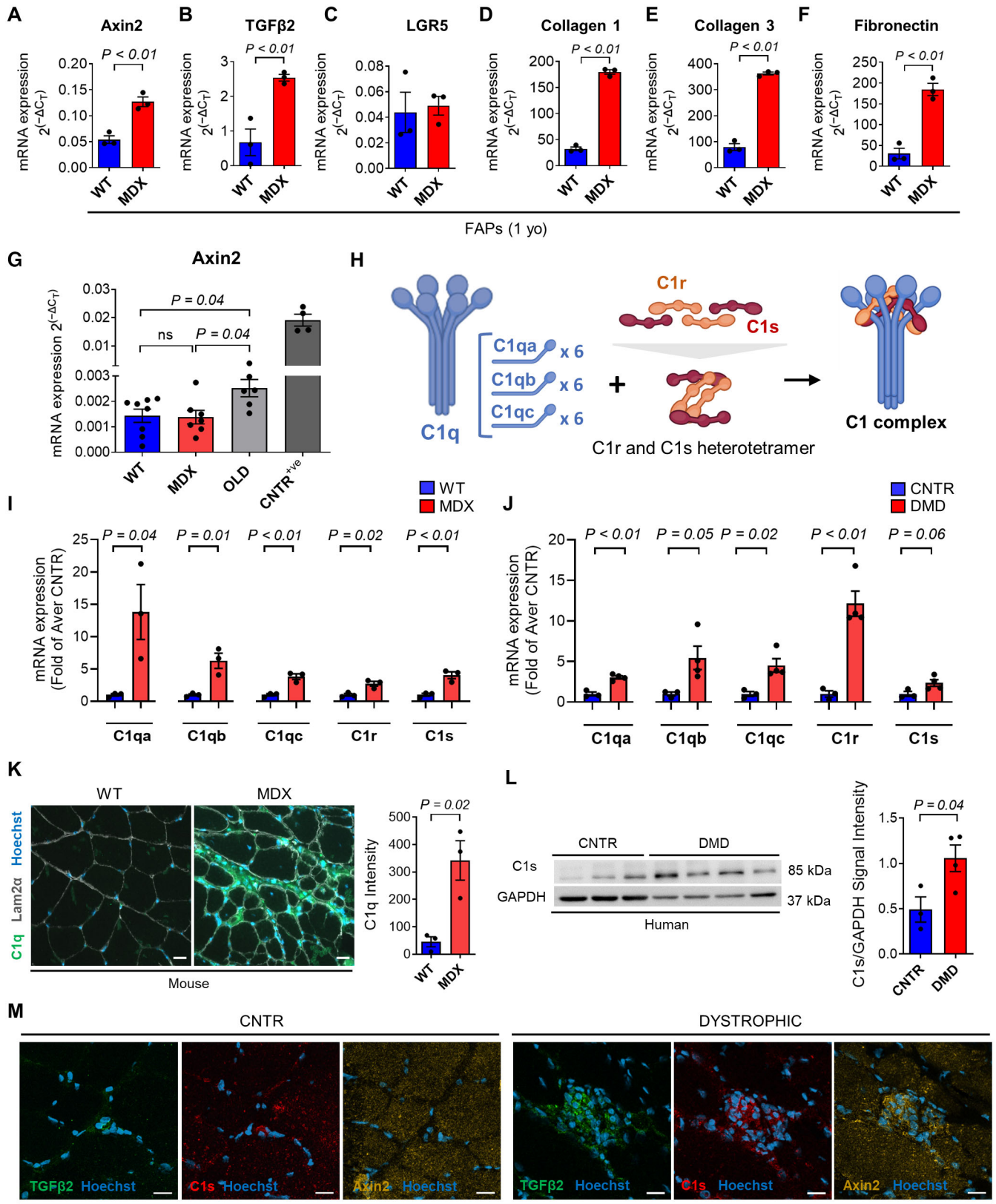


Figure 1.

Figure 1. C1 is locally produced by skeletal muscles and is enhanced in dystrophy.

- A–F *Axin2* (A), *TGFβ2* (B), *LGR5* (C), *collagen 1a1* (D), *collagen 3a1* (E), and *fibronectin* (F) mRNA expression in FACS-isolated FAPs from ~1-year-old *WT* and *MDX* hindlimb muscles. *N* (biological replicates) = 3.
- G *Axin2* mRNA expression in C2C12 cultured for 6 h in DMEM with 5% serum collected from ~7-months-old *WT*, ~7-months-old *MDX*, and ~2.5-years-old *WT* (OLD) mice or with 50 ng/ml WNT3A (CNTR^{+/ve}). *N* (biological replicates) = 8 (*WT*), 7 (*MDX*), 6 (OLD), and 4 (CNTR^{+/ve}).
- H Schematic representation of C1 protein complex. Created with BioRender.com.
- I, J *C1qa*, *C1qb*, *C1qc*, *C1r*, and *C1s* mRNA expression in hindlimb muscles of ~1-year-old *WT* and *MDX* mice (I) and biceps muscles of healthy controls (CNTR) and DMD patients (DMD) (J). *N* (biological replicates) = 3 (*WT*, *MDX*, CNTR) and 4 (DMD).
- K Representative immunofluorescence (left) and quantification (right) of C1q in the *gastrocnemius* of ~1-year-old *WT* and *MDX* stained with anti-C1q (green), anti-Laminin2α (gray) antibodies, and Hoechst (blue). Scale bar: 20 μm. *N* (biological replicates) = 3.
- L Western blot (left) and quantification (right) of C1s in human healthy (CNTR) and dystrophic (DMD) biceps muscles. *N* (biological replicates) = 3 (CNTR) and 4 (DMD).
- M Representative immunofluorescence of serial sections of human healthy (CNTR) and dystrophic (DMD) biceps muscles stained with anti-TGFβ2 (green), anti-C1s (red), anti-Axin2 (yellow), and Hoechst (blue). Note that TGFβ2, C1s, and Axin2 colocalize in the interstitial areas of DMD muscles. Scale bar: 20 μm.

Data information: Data are presented as mean ± SEM. In (K) each graph dot represents the average value of 9 to 44 measurements on different muscle regions for each biological sample. Statistical differences were calculated in G by one-way ANOVA test among *WT*, *MDX*, and *OLD* groups. Tukey's multiple-comparison test was used as a *post hoc* test. In (A–F) and (I–L), statistical differences were calculated by unpaired two-tailed Student's *t*-test. *P*-values are as indicated.

Source data are available online for this figure.

expression of the well-established transcriptional target of canonical WNT signaling *Axin2* was evaluated by quantitative PCR (Fig 1G). While *Axin2* expression was increased in cells cultured with the serum collected from ~2.5-years-old mice compared to the ~7-months-old *WT* and *MDX* mice, its expression in cells cultured with the *MDX* serum was not significantly different from cells cultured with the age-matched *WT* serum (Fig 1G). In line with this observation, only a negligible increase in the amount of C1q and C1s was observed in the *MDX* serum compared to the *WT* (Appendix Fig S2A and B). These data suggest that the events leading to increased WNT activity in dystrophic muscles differ from those occurring in aging tissues and likely do not depend on the release of complement C1 in the circulation. Therefore, we hypothesize that the increased WNT activity in dystrophic muscles could depend on the local production of molecules capable of initiating the WNT signaling pathway. We focused our attention on the complement C1 complex. C1 complex comprises C1q, which consists of C1qa, C1qb, and C1qc, and the heterotetramer C1s/C1r/C1r/C1s (Fig 1H). We found that all C1 components are actively transcribed in dystrophic muscles, and their mRNA levels are increased compared to the *WT* age-matched controls (Fig 1I). Importantly, a similar pattern was observed in muscles from human dystrophic patients (Fig 1J and Appendix Table S1). Moreover, C1q and C1s protein expression resulted higher in dystrophic mice muscles compared to the *WT* controls in our immunofluorescence analysis (Fig 1K and Appendix Fig S3A). The overexpression of C1s protein and the activation of the C1/WNT axis (i.e., C1s, Axin2, and TGFβ2 expression) were confirmed in muscle biopsies from dystrophic patients compared to healthy controls (Fig 1L and M). In keeping with the overexpression of all components of the C1 complex, we observed the deposition of C4, an event occurring downstream to C1, in the interstitial space of *MDX* muscles (Fig EV2A). Our ELISA assay confirmed the presence of increased amounts of C4 in dystrophic mice muscles compared to the *WT* age-matched counterparts (Appendix Fig S3B). These data indicate that the enhanced WNT signaling in the *MDX* mice is likely not caused by factors in the serum. The increased gene expression of C1 complex components in both dystrophic mice and patients suggests the local production of these proteins in the affected muscles.

Distinct cell types express different C1 components in muscles

To further corroborate the idea of a local overproduction of complement C1 in dystrophic muscles, we investigated which muscle cell type/s express each of the five C1 subunits. We fractionated by FACS the mononucleated cells in skeletal muscle in five distinct and not overlapping subfractions: macrophages, FAPs, MuSCs, Lin^{+/ve}F4/80^{-ve} cells (i.e., endothelial cells and cells of hematopoietic lineage with the exclusion of mature macrophages), and Lin^{-ve}Sca1^{-ve}VCAM^{-ve} cells (i.e., all the remaining muscle mononucleated cells) (Appendix Fig S4A). We also enzymatically dissociated the muscles to obtain single myofibers. The analysis on *MDX* muscles was performed in parallel with uninjured *WT* muscles and *WT* muscles undergoing regeneration after an acute injury to highlight unique aspects associated with the chronic condition of regeneration typical of DMD. Our quantitative PCR analysis showed that: (i) *C1qa*, *C1qb*, and *C1qc* are uniquely expressed by macrophages in all three conditions (i.e., *WT*, *MDX*, and *WT* after injury) (Fig 2A–C and Appendix Table S2); and (ii) *C1r* and *C1s* are mostly expressed by FAPs and to a minor extent by Lin^{-ve}Sca1^{-ve}VCAM^{-ve} cells in all three conditions (Fig 2D and E, and Appendix Table S3). The population-specific expression of C1 was confirmed at the protein level. C1q protein was observed in FACS-isolated F4/80^{+/ve} cells (macrophages) of *MDX* muscles through immunofluorescence but not in FAPs nor MuSCs isolated from the same muscles (Appendix Fig S5A). Moreover, the expression of C1q in macrophages was confirmed in *MDX* muscle sections (Appendix Fig S5B and C). Similarly, when we interrogated public human muscle transcripts datasets, C1q genes appeared uniquely expressed by macrophages, whereas C1r and C1s were enriched in *bona fide* FAPs (i.e., mesenchymal stem cells) (Appendix Fig S6A–F). We confirmed this pattern of expression at the protein level. C1q protein expression was higher in human hematopoietic cells (i.e., CD45^{+/ve}, which include macrophages) compared to FAPs (Appendix Fig S6G), whereas C1s protein expression was higher in human FAPs compared to both hematopoietic and endothelial cells (Appendix Fig S6H).

Intriguingly, our transcriptional analysis revealed also that: (i) *C1r* and *C1s* are less expressed in FAPs isolated from injured *WT* muscles compared to the *MDX* (Fig 2D and E); and (ii) *C1q* cluster genes are less expressed in macrophages isolated from injured *WT*

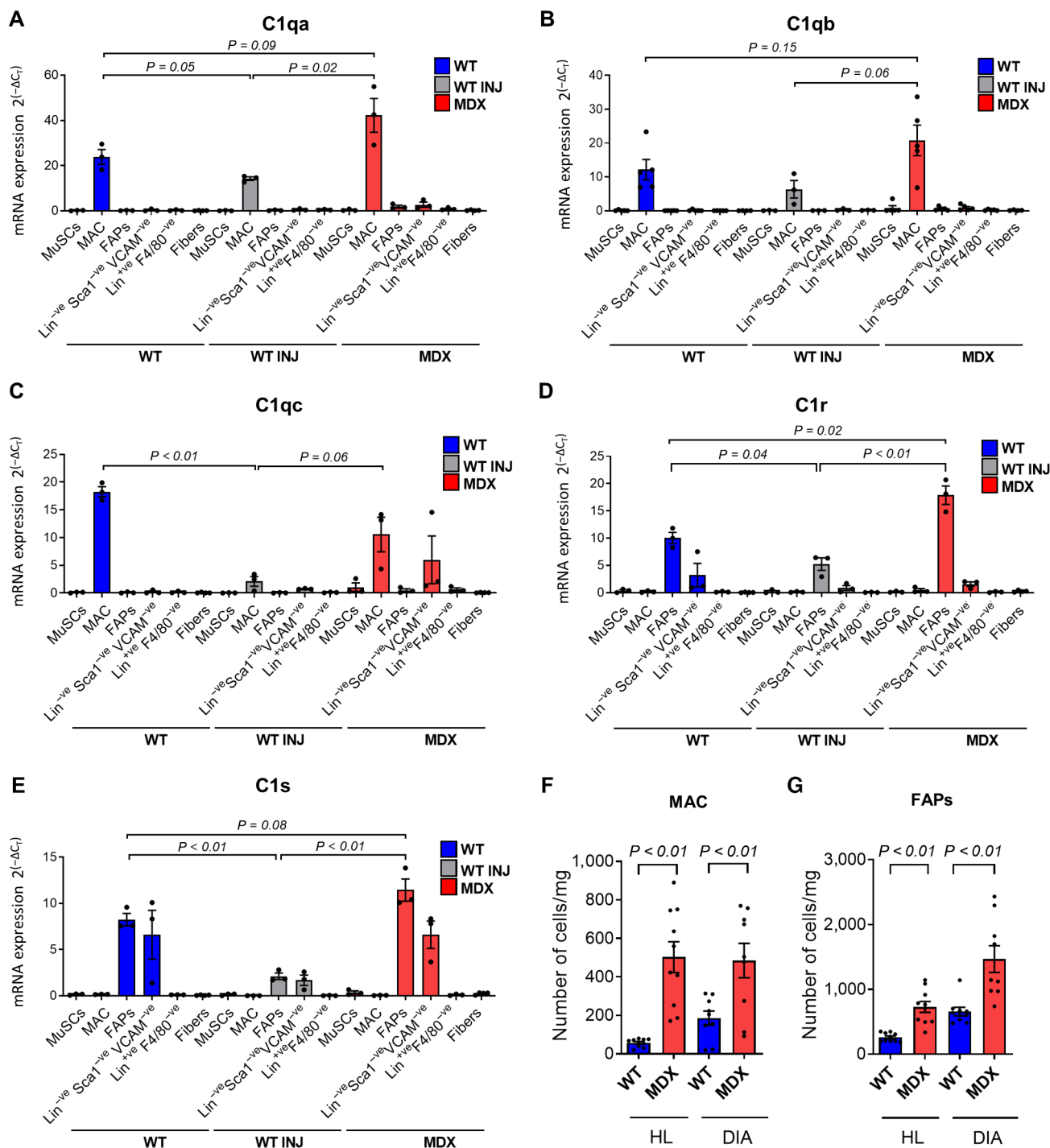


Figure 2. Distinct cell types express the C1 complex's components in the skeletal muscles.

A–E *C1qa* (A), *C1qb* (B), *C1qc* (C), *C1r* (D), and *C1s* (E) mRNA expression in MuSCs, macrophages (MAC), FAPs, *Lin*^{-ve}*Sca1*^{-ve}*VCAM*^{-ve}, *Lin*^{+ve}*F4/80*^{-ve}, and myofibers isolated from hindlimb muscles of ~1-year-old WT and MDX mice and muscles of WT mice 2.5 days after acute injury (WT INJ). *N* (biological samples) = 3 for all samples except for *C1qb* (*N* = 5) and fibers (*N* = 4).

F, G Number of macrophages (F) and FAPs (G) per mg of tissue in hindlimb (HL) and diaphragm (DIA) muscles of ~1-year-old WT and MDX mice. *N* (biological samples) = 10 (HL) and 9 (DIA).

Data information: Data are presented as mean ± SEM. In (A–E), statistical differences between two groups were calculated by unpaired two-tailed Student's *t*-test, and the corresponding *P*-values are reported on the graphs. Statistical differences between three or more groups were calculated by one-way ANOVA test, Tukey's multiple-comparison test was used as a *post hoc* test, and all the corresponding *P*-values are enclosed in Appendix Tables S2 and S3. In (F, G) statistical differences between two groups were calculated by unpaired two-tailed Student's *t*-test. *P*-values are as indicated.

Source data are available online for this figure.

muscles compared to the MDX, with *C1qa* expression reaching statistical significance and *C1qb* and *C1qc* exhibiting a trend (Fig 2A–C). Noteworthy, we found a similar expression of the cell proliferation marker gene *E2F1* in macrophages and FAPs isolated from MDX and injured WT muscles, suggesting that the differential C1 expression between dystrophic and acute degenerative conditions is unlikely depending on differences in the cellular proliferative state (Appendix Fig S7A) (Chen et al, 2009). In summary, different cell types within the skeletal muscles express the various C1 components. The cellular transcription of the C1 subunits is higher overall in dystrophic muscles than in muscles undergoing regeneration following a single acute injury event.

We next quantified the number of macrophages and FAPs to assess whether an increased number of these cell types may also contribute to the enhanced expression of complement levels in the dystrophic muscles (see Fig 1I–M, and Appendix Fig S3A and B). In agreement with previous reports, the number of both macrophages and FAPs was significantly increased in dystrophic muscles compared to the WT age-matched controls when calculated both as total number of cells per mg of tissue, as well as percentage, respectively, of CD45⁺CD31⁺ cells and CD45⁻CD31⁻ cells (Fig 2F and G, and Appendix Fig S8A and B) (Tidball & Villalta, 2010; Contreras et al, 2016). Altogether our evaluation of the complement levels both at the gene and protein levels suggests that the increased C1 expression in dystrophic muscles is due to a combination of two factors: (i) an increased number of macrophages and FAPs in the dystrophic muscles, with these two cell types being, respectively, the main cellular sources of C1qa/b/c/ and C1r/s; (ii) increased production by the FAPs (for *C1r* and *C1s*) and macrophage (for *C1q*) populations in the dystrophic compared to the injured WT environment.

Differentiated macrophages (F4/80⁺) are divided by functional and molecular criteria into several subpopulations (Tidball & Villalta, 2010; Wang & Zhou, 2022). Our immunofluorescence analysis suggests that high levels of the C1q subunits are expressed only by a fraction of the whole macrophage population (Appendix Figs S5 and S6). To gain insight into this aspect, we interrogated publicly available murine and human single-cell gene expression datasets and observed a correspondence between the fraction of

C1q-expressing macrophages and the subsets expressing CD163 or CD206 (Appendix Figs S6A–D and S9A–G). CD206 and CD163 are reportedly marking muscle-resident or anti-inflammatory subsets of macrophages (Villalta et al, 2009; Wang et al, 2020). Notably, the fraction of CD206⁺ macrophages expressing C1q appears to be distinct from the subset expressing the anti-inflammatory marker IL-10 (Appendix Fig S9H) (Purcu et al, 2022). To corroborate these observations, we FACS purified F4/80⁺ macrophages from dystrophic and acutely injured muscles, and we fractionated them based on the intensity of the CD206 staining (Fig EV3A and Appendix Fig S10A). Under both injury paradigms, CD206 is expressed in most macrophages, although with different intensities (Fig EV3B and Appendix Fig S10B). Notably, when we performed a gene expression analysis in the CD206⁻, CD206^{Low}, and CD206^{High} macrophages, we could observe that only in the dystrophic environment the enhanced CD206 and CD163 expression in the CD206^{Low/High} subfractions correlates with an increase in the transcription of *C1qa*, *C1qb*, and *C1qc* (Fig EV3D–H and Appendix Fig S10D–H). The analysis of IL-10, TNF α , and TGF β 1, which are, respectively, predominating in macrophages with anti-inflammatory, inflammatory, and profibrotic functions, suggests that the CD206-expressing macrophages in acutely injured muscles might be more anti-inflammatory compared to their dystrophic counterpart (Fig EV3I and J, and Appendix Fig S10I and J) (Tidball & Villalta, 2010; Wang & Zhou, 2022). Altogether, these observations suggest that C1q subunits might be preferentially expressed in a CD206⁺CD163⁺ subset of macrophages that is not anti-inflammatory and is enriched in dystrophic muscle.

C1 activates the WNT signaling in fibroblasts, myoblasts, and FAPs

We tested C1 expression in murine fibroblasts (i.e., STO, C3H-10T1/2, and NIH-3T3), macrophages (i.e., RAW-264.7), and myoblasts (i.e., C2C12 and primary myoblasts) in order to establish an *in vitro* model that recapitulates the differential expression of C1 components observed *in vivo*. Similar to our analysis of freshly isolated cells (Fig 2A–E, and Appendix Tables S2 and S3), we observed that *C1qa*, *C1qb*, and *C1qc* are mostly transcribed by macrophages

Figure 3. C1 activates the canonical WNT signaling in murine fibroblasts, myoblasts, and FAPs.

- A–C *C1qa* (A), *C1qb* (B), and *C1qc* (C) mRNA expression in cell lines as indicated (Mac: macrophages). *N* (independent experiments) = 3.
- D Representative immunofluorescence image of cells as indicated stained with an anti-C1q (green) antibody and Hoechst (blue). C1q protein is expressed selectively by macrophages. Scale bar: 10 μ m.
- E, F *C1r* (E) and *C1s* (F) mRNA expression in cell lines as indicated. *N* (independent experiments) = 3.
- G–I *Axin2* mRNA expression in STO (G, H) and C2C12 (I) cells cultured with STO-conditioned medium (STOm) or STOm+C1q for 6 (G) or 24 (H, I) hours. *N* (biological samples) = 3 (G, H), 6 (CNTR^{-ve} and STOm in I), 4 (STOm + C1q in I), and 2 (CNTR^{+ve} in I). CNTR^{+ve}: WNT3A 25 ng/ml in (G, H) and 100 ng/ml in (I). CNTR^{-ve}: cell medium plus reagents' solvents.
- J Scheme of the experiments shown in (K–M).
- K–N *Axin2* mRNA expression in C2C12 cells cultured with cell media (CNTR^{-ve}) or reagents as indicated for 24 (K, M), 6 (L), or 18 (N) hours. *N* (biological replicates) = 3 (K, M, STOm + RAWm, and STOm + RAWm + XAV in L), 4 (CNTR^{-ve} in L, C1q + C1r + C1s, and CNTR^{+ve} in N), 5 (CNTR^{-ve} in N), and 2 (CNTR^{+ve} and WNT3A + XAV in L). XAV: XAV939, INHr/s: C1r/s inhibitor. CNTR^{-ve}: cell medium plus reagents' solvent. CNTR^{+ve}: WNT3A 100 ng/ml (K) and 50 ng/ml (L, N).
- O *Axin2* mRNA expression in FAPs freshly FACS isolated from WT mice 8 days after cardiotoxin injury and cultured with cell media (CNTR^{-ve}) or reagents/inhibitors as indicated for 24 h. *N* (biological replicates) = 7 (except for CNTR^{-ve}, *N* = 4). CNTR^{-ve}: cell medium plus reagents/inhibitors' solvent. CNTR^{+ve}: WNT3A 100 ng/ml.

Data information: In (A–C), (E–I), and (K–O), data are presented as mean \pm SEM. Statistical differences between three or more groups were calculated by one-way ANOVA test, and Tukey's multiple-comparison test was used as a *post hoc* test. The statistics were calculated by paired two-tailed Student's *t*-test in (M) and by unpaired two-tailed Student's *t*-test in (N). *P*-values are as indicated.

Source data are available online for this figure.

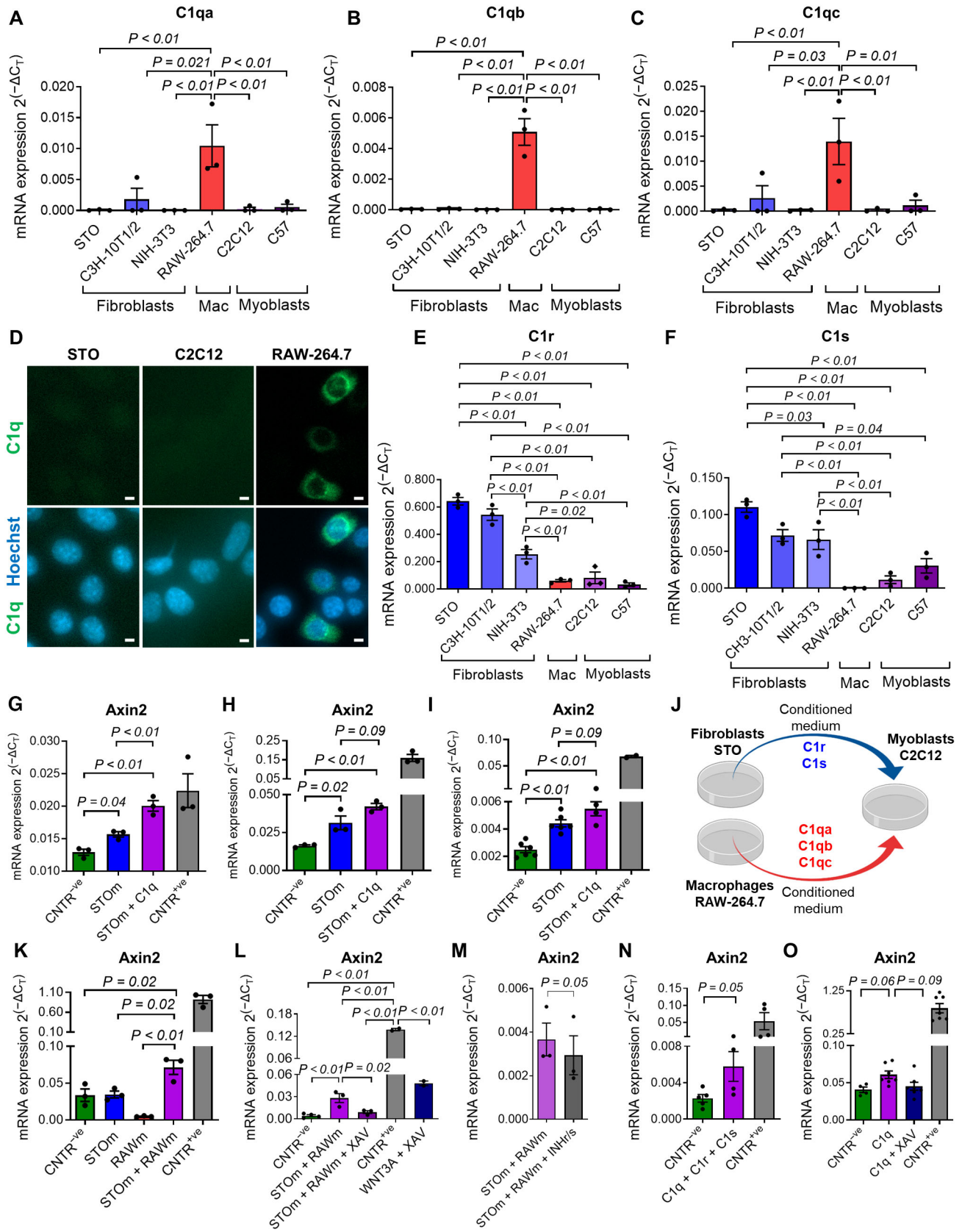


Figure 3.

(Fig 3A–C); C1q protein expression was observed through immunofluorescence in a fraction of macrophages, but not in fibroblasts, nor in myoblasts (Fig 3D). *C1s* and *C1r* are mostly expressed by fibroblasts (Fig 3E and F), and myoblasts express only traces of all C1 components (Fig 3A–C, E and F).

We next studied C1-mediated modulation of the canonical WNT signaling *in vitro* in three different cell types: (i) fibroblasts, which express high levels of C1s and C1r similarly to the FAPs in muscles (Fig 3E and F), (ii) myoblasts that express low levels of C1 similarly to satellite cells and myofibers (Fig 3A–F), and (iii) muscle-isolated FAPs. All C1 subunits are secreted proteins (Gulati et al, 1994). We used fibroblasts' (STO) and macrophages' (RAW-264.7) conditioned media (expected to be, respectively, enriched in C1r/C1s and C1q proteins) to treat STO fibroblasts and C2C12 myoblasts. An increased expression of *Axin2* was observed in STO treated with STO medium supplemented with recombinant C1q compared to cells treated with STO medium alone or with the unconditioned medium (Fig 3G and H). An analogous trend was observed when C2C12 was treated similarly (Fig 3I). An increased expression of *Axin2* was also observed in C2C12 myoblasts treated with the combination of STO and RAW-264.7 media compared to the same cells treated with just one of the two media (Fig 3J and K). *Axin2* increased expression was rescued in C2C12 cells treated with XAV-939, a well-known inhibitor of canonical WNT signaling (Fig 3L). A partial but statistically significant reduction was observed when a C1 inhibitor was added, indicating that at least part of the WNT activity depends on C1 components secreted in the media (Fig 3M). Myoblasts were treated with recombinant C1q, C1r, and C1s proteins, and an increased level of *Axin2* was observed compared to the cells cultured with the control solution, further suggesting that C1 might be the factor leading to an increased WNT signaling in these cells (Fig 3N). Finally, the supplementation of C1q was able to increase *Axin2* expression also in muscle-isolated FAPs, and the addition of XAV-939 blocked this response (Fig 3O). Altogether, these *in vitro* observations suggest that the formation of the C1 complex has the potential to enhance the activity of the canonical WNT signaling in various cell types, including FAPs. These data further support the idea that the different subunits of the C1 complex are released by different cell types and act as a combinatorial source of WNT signaling.

Increased macrophages, FAPs, and C1/WNT axis in the MDX

In order to get insights into the possibility that macrophages and FAPs may act in combination to induce WNT signaling *in vivo*, we first studied the localization of FAPs and macrophages within the dystrophic muscles. Both these cells are required for the formation of C1 as they, respectively, release C1r/s and C1q. They are, therefore, expected to be physically close in the MDX-regenerating foci. To identify FAPs, we used the *PDGFR α ^{eGFP}* reporter strain that has the H2B-eGFP fusion protein knocked into the *PDGFR α* locus and has been previously used to mark FAPs in muscles (Mueller et al, 2016). Our FACS and immunofluorescence analysis performed on muscles collected from *PDGFR α ^{eGFP/WT};MDX* mice confirmed that the eGFP⁺ population overlaps with the interstitial FAPs cell population (Appendix Fig S11A and B). Muscles from dystrophic *PDGFR α -eGFP;MDX* males were stained with anti-F4/80 antibody to mark macrophages, and the distance between macrophages and FAPs was measured (Fig 4A). Muscles from *PDGFR α ^{eGFP/WT};MDX^{+/-}* heterozygous female carriers and non-dystrophic *PDGFR α ^{eGFP/WT}* mice were used as asymptomatic controls (Fig 4A). Clusters of macrophages and FAPs were observed in the muscle areas characterized by high cellularization (i.e., in *bona fide* regenerative foci) of the dystrophic *PDGFR α ^{eGFP/WT};MDX* males (Fig 4B). Both macrophages-to-FAPs and FAPs-to-macrophages distances were measured, demonstrating that macrophages and FAPs are closer to each other in dystrophic muscles than in controls (Fig 4A and Appendix Fig S11C–F). Moreover, dystrophic *PDGFR α ^{eGFP/WT};MDX* muscles showed a higher percentage of macrophages and FAPs direct contacts compared to the controls (Fig 4B and C).

We showed in this study that macrophages and FAPs are increased in dystrophic muscles and near each other in the regenerative foci of dystrophic muscles, where they can potentially promote WNT activity by secreting distinct subunits of the C1 complex. To corroborate this view, we investigated whether the increased presence of these cells correlates with the enhanced WNT signaling activity. We found an increased expression of the profibrotic WNT-target TGF β 2 in the regenerating areas of dystrophic mice, which were also characterized by an increased number of macrophages and FAPs compared to the non-dystrophic controls (Appendix Fig S12A; Biressi et al, 2014). Similar to TGF β 2, we also found that

Figure 4. Enhanced C1/WNT axis in the dystrophic regenerating foci.

- A Distance (μ m) between macrophages (MAC) and FAPs in *gastrocnemius* of ~12-months-old male *PDGFR α ^{eGFP/WT}* (CNTR WT), ~18-months-old female *PDGFR α ^{eGFP/WT};MDX^{+/-}* (CNTR HET), and ~18-months-old male *PDGFR α ^{eGFP/WT};MDX* (MDX) mice. The analysis was performed by measuring the distance of each macrophage in the image field from its closest FAP. *N* (biological replicates) = 3 (CNTR HET, MDX) and 1 (CNTR WT).
- B Representative immunofluorescence of a *bona fide* regenerating area in the *gastrocnemius* of a ~18-months-old male *PDGFR α ^{eGFP/WT};MDX* mouse stained with anti-F4/80 (red), anti-eGFP (green) antibodies, and Hoechst (blue). White arrows indicate contacts between macrophages (F4/80⁺) and FAPs (eGFP⁺). Scale bar: 20 μ m.
- C Percentage of contacts (i.e., distance of 3 μ m or less) between macrophages and FAPs calculated in same muscles as in (A). *N* (biological replicates) = 3 (CNTR HET, MDX) and 1 (CNTR WT).
- D, E Representative immunofluorescence of *gastrocnemius* of ~1-year-old MDX stained with anti-C1q (red), anti-Axin2 (green in D), anti-TGF β 2 (green in E) antibodies, and DAPI (blue). Scale bar: 100 μ m (low-magnification images) and 20 μ m (high-magnification images). The positive correlation between C1q and Axin2 (D) and C1q and TGF β 2 (E) intensity values is shown. *N* (biological replicates) = 3.

Data information: In (A) data are presented as median with interquartile range. Each dot on the graph represents a distance measurement (86 for WT, 335 for CNTR HET, and 827 for MDX). Statistical differences were calculated by the Kruskal–Wallis test. Dunn's multiple-comparison test was used as a *post hoc* test. In (C) data are presented as mean \pm SEM. Statistical differences between CNTR HET and MDX groups were calculated by unpaired two-tailed Student's *t*-test. In (D and E) each graph dot represents a measurement of a muscle area (196 in D and 289 in E). The positive correlation between C1q and Axin2/TGF β 2 was assessed using two-tailed correlation test and computing the Spearman coefficient (*r*) for Axin2 (in D) or TGF β 2 (in E) versus C1q dataset. *P*-values are as indicated. Source data are available online for this figure.

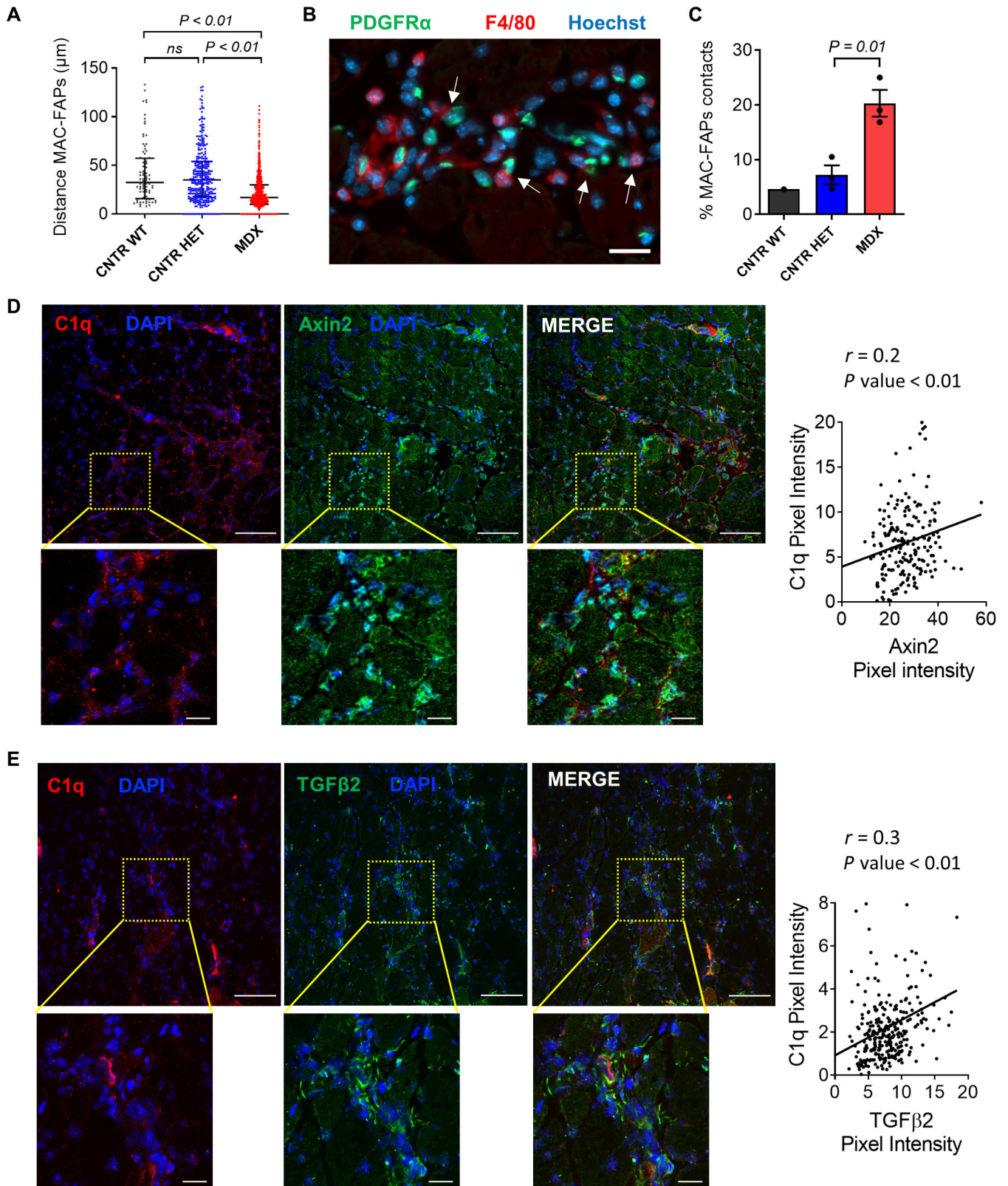


Figure 4.

the canonical WNT signaling effectors/target proteins β -catenin colocalize with F4/80⁺ cells in the regenerating areas of MDX muscles (Appendix Fig S12B and C). Moreover, regions within the regenerating areas of MDX muscles that were characterized by strong expression of Axin2 or TGF β 2 also exhibited a strong expression of C1q protein (Fig 4D and E). The positive correlation between C1q/Axin2 and C1q/TGF β 2 intensities is consistent with the possibility that the augmented complement contributes to the increased WNT/TGF β axis reported in dystrophy (Biressi et al, 2014).

Increased WNT signaling and fibrosis in the fib-MDX mouse FAPs

The fib-MDX mouse model is a dystrophic mouse that overcomes some limitations associated with the mild pathological phenotype of the MDX mice compared to the human disease (Desguerre et al, 2012; McGreevy et al, 2015). To get access to muscles that closely recapitulate the severity of the human pathology, we tested the fib-MDX mouse model by performing daily micro-injuries in the distal muscles of the hindlimb of MDX mice for 2 weeks (Fig 5A). This procedure leads to a dramatic alteration of muscle histology and deposition of interstitial collagen (Fig 5B and Appendix Fig S13A). Notably, we could observe the accumulation of FAPs in the collagen-rich interstitium of the fib-MDX muscles (Appendix Fig S13B). To investigate the C1/WNT axis in the fib-MDX mouse model, we quantified the number of C1-producing cells. The number of both FAPs and macrophages was increased in the fib-MDX compared to the uninjured MDX muscles (Fig 5C and D, and Appendix Fig S13C and D). This increment parallels a further increase in the proximity between FAPs and macrophages in the fib-MDX model in comparison to the classic MDX and to acutely cardiotoxin-injured WT muscles (Fig EV4A–D). Moreover, when we isolated FAPs from the fib-MDX, we could observe an increase in the transcription of C1r and C1s subunits compared to the classic MDX mice (Fig 5E and F). A similar result was also obtained with the three C1q subunits in F4/80⁺ macrophages (Fig 5G–I). Intriguingly, when we further characterized macrophages from the fib-MDX for the expression of known heterogeneity markers, we could observe not only a general shift toward a more proinflammatory phenotype (i.e., characterized by a predominance of TNF α) compared to the classic MDX but also an upregulation of CD206 and CD163 that are marking a fraction of macrophages enriched for C1q expression in dystrophic muscle (Fig EV4E–H).

Next, we wondered if the increase in C1-producing cells and the increment in the expression of C1 subunits observed in the fib-MDX model could lead to enhanced activation of the WNT signaling pathway and fibrogenic program. FAPs and MuSCs were FACS isolated

1 week after the last injury and analyzed for the expression of both canonical WNT signaling targets (i.e., *Axin2*, *TGF β 2*, and *LGR5*) and fibrosis-related genes (i.e., *collagen1a1* and *collagen3a1*). Interestingly, *Axin2*, *LGR5*, *collagen 1a1*, and *collagen 3a1* transcripts were strongly increased in the FAPs of the fib-MDX muscles compared to the classic uninjured MDX muscles (Fig 5J–N). Only a trend was observed in the expression of TGF β 2, *collagen 1a1*, and *collagen 3a1* in MuSCs (Appendix Fig S14C–E). Moreover, immunofluorescence analysis revealed that the percentage of FAPs expressing the profibrotic WNT-target TGF β 2 was increased in the fib-MDX model (Fig EV4I). On the one hand, these data are in line with increased inflammation, the augmented activity of the C1/WNT axis and extracellular matrix deposition, and a more severe dystrophic phenotype occurring in fib-MDX mouse model compared to the classical MDX mice (Desguerre et al, 2012). On the other hand, these observations candidate the fib-MDX mice as a valuable model to study the profibrotic role of FAPs.

To get further insights into the nature of the cells responsive to the C1q-mediated induction of the WNT signaling in dystrophic muscle, we tested the expression of the WNT co-receptor LRP6, which reportedly mediates the C1-dependent activation of the WNT signaling pathway in aging (Naito et al, 2012). LRP6 was found to be expressed in MuSCs, macrophages, FAPs, Lin^{-ve}Sca1^{-ve}VCAM^{-ve}, Lin⁺F4/80^{-ve}, and isolated fibers, both in the WT and dystrophic muscles (Appendix Fig S14F). However, despite MuSCs and FAPs expressing comparable amounts of TGF β 2 (Appendix Fig S14G), FAPs had the highest expression of LRP6 among all the dystrophic cells, suggesting their major contribution to the enhanced canonical WNT signaling in dystrophy (Appendix Fig S14F). In line with its expression in freshly isolated cells, LRP6 was also more expressed in fibroblasts (STO and C3H-10T1/2) compared to myoblast (C2C12) cell lines (Appendix Fig S14F). Altogether, these observations ascribe to FAPs a central role in the profibrotic events that are operating downstream to the C1/WNT axis in muscular dystrophy, as revealed by the fib-MDX model.

C1r/s inhibition alleviates dystrophy in the fib-MDX model

Our findings suggest that inhibiting complement C1 might be a way to counteract the aberrant behavior of FAPs in the muscles of dystrophic mice. To directly test this possibility, we systemically administered to the fib-MDX mice a C1r/s inhibitor (Fig 6A). The gene expression analysis of FACS-isolated FAPs from muscles revealed a reduced expression of both the canonical WNT signaling targets (i.e., *Axin2*, *LGR5*, and *TGF β 2*) and the fibrogenic genes (i.e., *collagen 1a1* and *collagen 3a1*) in the fib-MDX mice after the complement

Figure 5. The fib-MDX mouse is a valuable model for studying FAPs in dystrophy.

- A Scheme of the generation of the fib-MDX mouse model.
- B Representative immunofluorescence image of a *gastrocnemius* of a ~1-year-old MDX and fib-MDX stained with anti-collagen 1 (yellow), anti-laminin 2 α (red) antibodies, and Hoechst (blue). Scale bar: 50 μ m.
- C, D Number of FAPs (C) and macrophages (D) per mg of tissue in the hindlimb of fib-MDX or uninjured MDX muscles. *N* (biological samples) = 3.
- E–I *C1r* (E), *C1s* (F), *C1qa* (G), *C1qb* (H), and *C1qc* (I), mRNA expression in FAPs (E, F) and macrophages (G–I) FACS isolated from fib-MDX or uninjured MDX hindlimb muscles. *N* (biological samples) = 4 (for all samples except MDX C1qa and MDX C1qb, *N* = 5).
- J–N *Axin2* (J), *LGR5* (K), *TGF β 2* (L), *collagen 1a1* (M), and *collagen 3a1* (N) mRNA expression in FAPs FACS isolated from fib-MDX or uninjured MDX hindlimb muscles. *N* (biological samples) = 3.

Data information: In (C–N) data are presented as mean \pm SEM. Statistical differences were calculated by unpaired two-tailed Student's *t*-test. *P*-values are as indicated. Source data are available online for this figure.

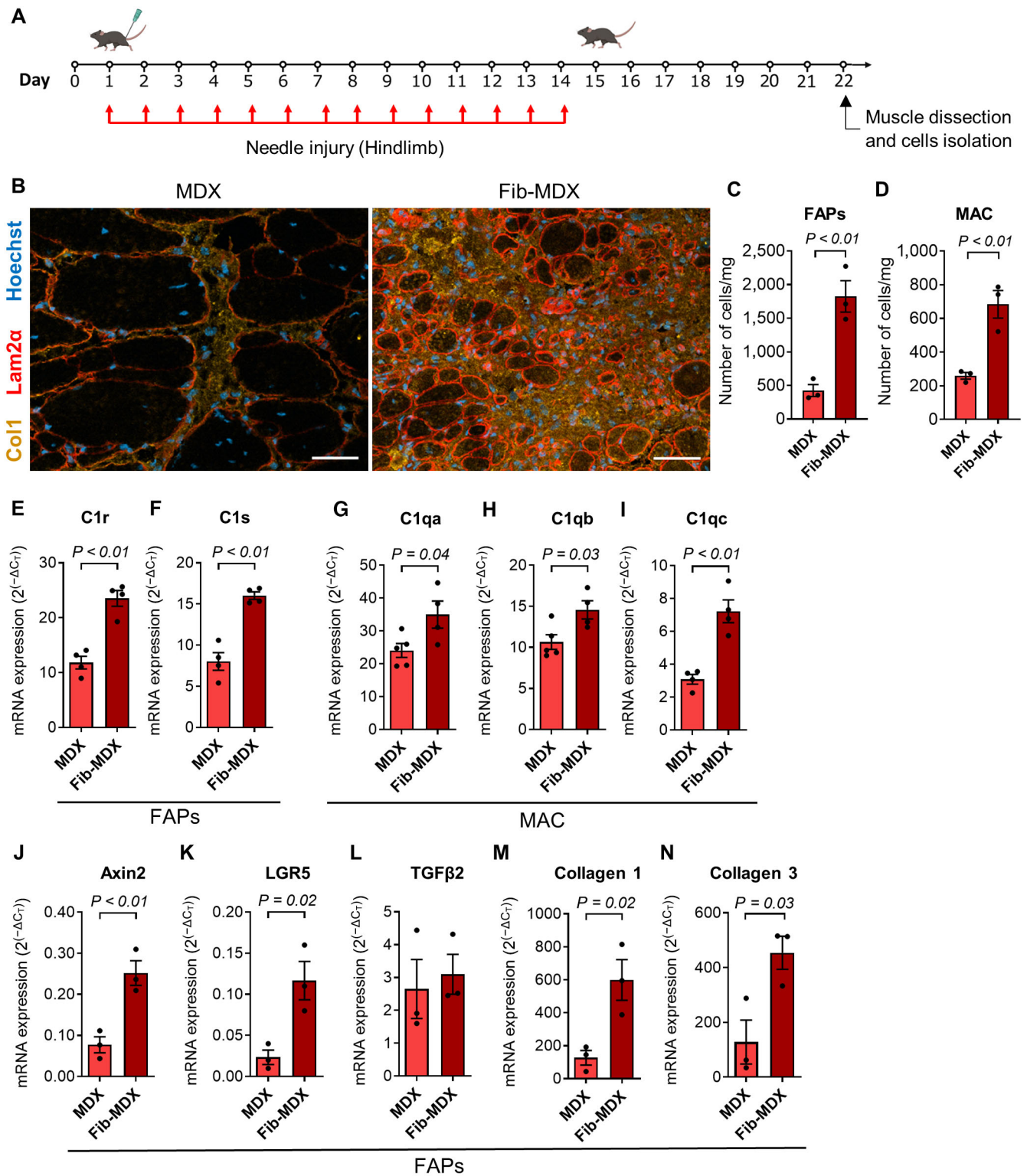


Figure 5.

inhibition (Fig 6B–F). Moreover, the intensity of the staining for TGF β 2 and the intracellular fibrotic marker HSP47 was reduced in FAPs in the muscles of the fib-MDX mice treated with the complement inhibitor (Appendix Fig S15A and B). The inhibition of the

fibrotic program associated with the WNT signaling appears to be FAPs specific, as it is not similarly altered in MuSCs (Appendix Fig S15C–G). Importantly, the muscles of the C1r/s inhibitor-treated fib-MDX mice presented a reduced space filled by fibrotic tissue

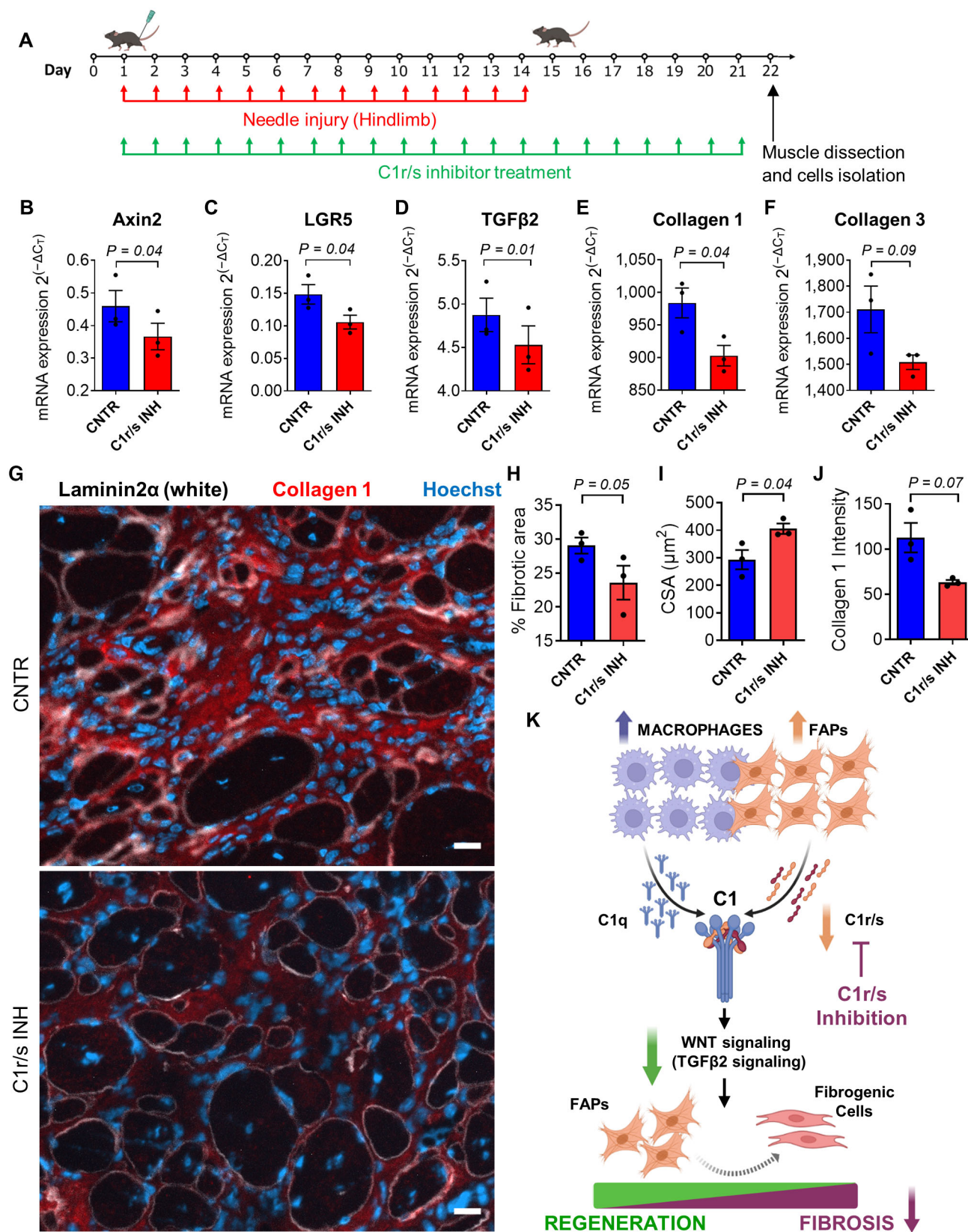


Figure 6.

Figure 6. *In vivo* inhibition of C1r/s rescues the dystrophic FAPs phenotype.

- A Scheme of the C1r/s inhibition experiment in the fib-MDX mice.
 B–F *Axin2* (B), *LGR5* (C), *TGF β 2* (D), *collagen 1a1* (E), and *collagen 3a1* (F) mRNA expression in FACS-isolated FAPs from ~1-year-old MDX mice processed as in (A). *N* (biological samples) = 3.
 G Representative immunofluorescence of *gastrocnemius* muscles from ~1-year-old MDX mice processed as in (A). Muscles were stained with anti-collagen 1 (red), anti-laminin 2 α (white) antibodies, and Hoechst (blue). Scale bar: 50 μ m.
 H Fibrotic area quantification of the same muscles as in (G). *N* (biological samples) = 3.
 I Cross-sectional area (CSA) quantification of the muscle fibers of the same muscles as in (G). *N* (biological samples) = 3.
 J Collagen 1 pixel intensity quantification in the interstitial space between myofibers of the same muscles as in (G). *N* (biological samples) = 3.
 K Model of the mechanism through which the C1/WNT axis affects FAPs in dystrophic muscles. C1r/s subunits are indicated as pharmacological targets for the effective inhibition of fibrosis. Created with [BioRender.com](https://www.biorender.com).

Data information: In (B–F) and (H–J), data are presented as mean \pm SEM. In (H and J), each graph dot represents the average value of 144 to 904 (H) and 17 to 27 (J) measurements on different muscle regions for each biological sample. In (I) each graph dot represents the median value of 201 to 372 cross-sectional area measurements on different muscle regions for each biological sample. Statistical differences were calculated by paired two-tailed Student's *t*-test. *P*-values are as indicated.

Source data are available online for this figure.

(Fig 6G and H), which paralleled an increased mean cross-sectional area of myofibers (Fig 6I). Moreover, the histological analysis revealed a decreased deposition of collagen in the interstitial space between myofibers in the muscles treated with the C1r/s inhibitor compared to the controls (Fig 6G and J, and Appendix Fig S15H and I). Altogether, these data highlight an amelioration of the dystrophic phenotype following the inhibition of the classical complement pathway (Fig 6K).

Despite being both dystrophy and acute injury characterized by a pronounced infiltration of inflammatory cells, the repertoire of macrophages appears different in the two conditions in terms of C1q expression (see Fig EV3F–H and Appendix Fig S10F–H). We decided to gain insight into this diversity by injecting the hindlimb muscles of *WT* mice with cardiotoxin and administering the same C1r/s inhibitor regimen that we have used in the fib-MDX mice (Fig EV5A). Eight days after injury, we collected the muscles from both treated and control animals and FACS-isolated FAPs and macrophages. As expected from the analysis performed at an earlier time point after injury (see Fig 2A–E), the five C1 subunits tend to be transcribed less in cells isolated from the acutely injured muscles compared to those isolated from the dystrophic fib-MDX (Fig EV5B–F). Intriguingly, this reduction parallels a shift toward an anti-inflammatory phenotype (i.e., characterized by a predominance of IL-10 expression) of the macrophages and a reduction in the expression of CD206 and CD163 (Appendix Fig S16A–D). Importantly, in contrast to what we observed in the fib-MDX model, the C1r/s inhibitor is not changing the expression of the WNT-target genes and collagens in FAPs isolated from acutely injured *WT* muscles (Fig EV5G–K). Moreover, despite the increase in fiber size, the accumulation of fibrotic tissue is not significantly altered by the administration of the C1r/s inhibitor (Fig EV5L–O). These observations disclose intrinsic differences in the process leading to fibrosis in physiological and dystrophic settings and highlight a peculiar detrimental profibrotic role played by the complement C1/WNT axis in dystrophic muscle (Appendix Fig S17).

Discussion

Our data link the enhanced local production of the five subunits of the C1 complex by macrophages and FAPs in dystrophic muscles

with enhanced WNT signaling and activation of a fibrogenic program in FAPs. Here, we present direct evidence that C1, the upstream component of the classical complement cascade, contributes to the etiology of fibrosis in the muscle affected by DMD.

So far, the involvement of the complement system in the etiology of fibrosis in DMD has been unexplored, being the complement system historically investigated in the process of myofiber necrosis (Engel & Biesecker, 1982; Sewry *et al*, 1987; Spuler & Engel, 1998). The presence of the membrane attack complex, complement C3, C8, and C9 was described in the necrotic fibers of DMD patients, but lack of clarity remains whether complement plays a causative role during the processes leading to fiber damage or is recruited after membrane lesions have already appeared (Sewry *et al*, 1987). Notably, whereas complement components commune to all complement pathways were associated with necrotic fibers, the presence of C1q and C4 was reported to be highly variable in the necrotic areas (Engel & Biesecker, 1982). This observation suggests the predominant involvement of the C1-independent alternative pathway in the process of necrosis in DMD. Further investigation will be required to understand if the classic complement pathways may also play a role in this context.

We propose that FAPs and macrophages, typically relatively distant in uninjured muscles, invade the regenerative areas of dystrophic muscle and locally secrete distinct complement C1 subunits that combine to induce the WNT-dependent fibrotic program. This model appears to differ from the one described to explain WNT-dependent defective regeneration in aging muscle, which likely depends on C1q circulating in the bloodstream (Naito *et al*, 2012). The reduced WNT activity that we report here for the serum collected from the dystrophic animals compared to the old *WT*, together with the similar WNT activity and amount of C1q present in the serum of dystrophic and age-matched *WT* mice, supports this view (see Fig 1G and Appendix Fig S2A). We could observe a moderate, although non-statistically significant, increase in C1s in the serum of MDX mice compared to the age-matched *WT* counterpart (Appendix Fig S2B). Additional studies are needed to conclusively evaluate if C1r/s might appear in the dystrophic subjects' bloodstream, possibly by spilling over from diseased muscles. Intriguingly, reduced levels of circulating C1r/s inhibitor have been reported in dystrophic patients (Nagao *et al*, 1987). This observation calls for an investigation of the levels of C1r/s inhibitor in aging and

further supports our idea of using C1r/s inhibitor as a pharmacological tool in DMD.

Our study does have some limitations. Although our analysis showed a clear reduction in fibrosis upon C1r/s inhibitor administration, the fib-*MDX* model that we used does not allow for a long-term (>3 weeks) functional evaluation. Furthermore, evidence indicates that macrophages consist of heterogeneous populations, which can be discriminated on the preferential involvement during specific phases of the regenerative response or their anatomical origin (i.e., muscle resident or recruited from the circulation) (Tidball & Villalta, 2010; Wang *et al.*, 2020; Babaeijandaghi *et al.*, 2022). Our data indicate a preferential expression of C1q in a specific macrophage subpopulation dominating the dystrophic muscle and characterized by expression of CD206 and CD163 (see Fig EV3). Nevertheless, the origin of this subpopulation, its relationship with other macrophage subpopulations, and its role during physiological and pathological muscle regeneration remain largely undisclosed and call for future in-depth characterizations. A similar investigation can be put forward for C1r/s expression in FAPs, which also are reportedly heterogeneous (Farup *et al.*, 2021).

Another aspect requiring additional investigation concerns the influence of the complement C1/WNT axis on the behavior of the MuSCs. Previous reports indicate that the activation of the WNT signaling pathway promotes TGF β signaling and that MuSCs acquire a fibrotic phenotype in a TGF β -dependent manner in the dystrophic environment (Biressi *et al.*, 2014; Pessina *et al.*, 2015). Nevertheless, the pharmacological inhibition of C1r/s in the fib-*MDX* model inhibited the WNT signaling and the fibrogenic program in FAPs but not in MuSCs. This difference could depend on features of the fib-*MDX* model that is magnifying the C1/WNT fibrogenic axis only in FAPs (Fig 5J–N and Appendix Fig S14A–E), or it may depend on intrinsic properties of the MuSCs that present a relatively low expression of the co-receptor LRP6 (Appendix Fig S14F), and possibly depend on complement-independent molecular mechanisms to activate the TGF β -mediated fibrogenic program.

Fibrosis contributes to the symptomatology of DMD and is a barrier to effective therapies (particularly for cell and gene therapy approaches) (Biressi *et al.*, 2020). By increasing our understanding of the mechanisms leading to fibrosis and attempting to interfere with them pharmacologically, this study strives to identify novel therapeutic avenues to ameliorate the condition of DMD patients. Given its upstream position in inflammation, complement C1-targeting drugs are in use for various rare diseases, and some hold orphan drug status (Reis *et al.*, 2015). Different pharmaceutical companies have clinical programs for antibodies blocking C1 subunits to treat cold agglutinin disease, Guillain-Barré Syndrome, and Huntington's disease (Jäger *et al.*, 2019). Inhibitors of C1r/s obtained as recombinant proteins or from human plasma, as used in our *in vivo* studies, are available in the clinic with a primary indication for the treatment of hereditary angioedema (Feussner *et al.*, 2014). This study explored the possibility of using these drugs to improve the condition of DMD patients.

An increased number of macrophages, high WNT signaling activity, and fibrosis are reportedly associated with cardiac dysfunction (Epelman *et al.*, 2015; Tao *et al.*, 2016). This aspect is relevant for DMD patients, as cardiac complications may be lethal in dystrophic patients (Finsterer & Stöllberger, 2003). Moreover, a chronic condition of inflammation, complement deposition, and enhanced

WNT signaling characterize many unrelated pathological conditions, including hypertensive arterial remodeling associated with atherosclerosis (Sumida *et al.*, 2015). Future studies will ascertain if the relevance of our findings extends beyond DMD muscle.

Materials and Methods

Mice

C57BL/6J mice (No. 000664, used as *wild-type* animals and herein referred to as *WT*), *B6Ros.Cg-D^{mdmdx-4Cv}/J* mice (No. 002378, herein referred to as *MDX*), and *B6.129S4-PDGFR α ^{tm11(EGFP)Sor/J}* reporter mice (No. 007669, herein referred to as *PDGFR α ^{EGFP}*) were purchased by The Jackson Laboratories. *PDGFR α ^{EGFP/WT};MDX* mice were obtained after breeding *PDGFR α ^{EGFP/WT}* males with *MDX* homozygous females (Mueller *et al.*, 2016).

Muscle needle injuries were performed using 29-gauge needles. Punctures were performed deep into the muscle (~8 mm), randomly but close enough to each other to cover the whole muscle. Muscles were dissected and analyzed 2.5 days after the injury. The fib-*MDX* mouse model generation protocol was adapted from a previously published protocol (Desguerre *et al.*, 2012). Briefly, 150- μ m-diameter micropins were used to perform 15 punctures in the *tibialis anterior* and 90 punctures in the *gastrocnemius* muscles daily for 14 days. Muscles were dissected and analyzed 1 week after the last injury. For complement inhibition, fib-*MDX* mice were treated with 15 UI of human plasma-derived C1r/s esterase inhibitor (Berinert, provided by CSL Behring) daily ~30 min after performing the microinjuries. C1r/s inhibitor was administered through intraperitoneal or intravenous injections on alternate days for 21 days starting from the first day of microinjuries. For specific experiments, muscle injury was performed by intramuscular injection of cardiotoxin from *Naja pallida* snake venom (Latoxan) resuspended at the concentration of 0.1 mg/ml in PBS 4 or 8 days before hindlimb muscle collection. For complement inhibition during physiological muscle regeneration, *WT* mice were treated with 15 UI of human plasma-derived C1r/s esterase inhibitor (Berinert) after the cardiotoxin injection and for the following 7 days. The following day, the hindlimb muscles were collected and processed for analysis.

Animal care and experimental procedures were conducted in accordance with the Ethical Committee of the University of Trento and were approved by the Italian Ministry of Health (Authorization Nos. 915/2015-PR and 94/2022-PR).

Protein analysis

Snap-frozen dissected muscles were homogenized and lysed with RIPA buffer (Thermo Scientific), protease inhibitor (1:100, Thermo Scientific), and phosphatase (1:100, New England BioLabs). The protein concentration was quantified using Pierce BCA Protein Assay Kit (Thermo Scientific). Standard indirect ELISA assays were performed on mice muscles and on mice sera. Anti-LGR5 (Abcam 219107, 1:500), anti-C4 (Santa Cruz 58930, 1:100), anti-C1s (LS-C483829 1:50), and anti-C1q (Abcam 182451 1:50) antibodies were used. Alkaline phosphatase-conjugated secondary antibodies (Life Technology) and p-nitrophenyl phosphate (Sigma) solution were used for the colorimetric assay at 405 nm (Tecan infinite M200

reader and Ensign reader). Background obtained with the secondary antibody was subtracted. Human muscle lysates were resolved by SDS-PAGE and transferred to PVDF membrane (Amersham™ Hybond™, Fisher Scientific). The membranes were blocked with 5% non-fat dry milk in TBS-T (50 mM Tris-HCl, pH 7.5, 150 mM NaCl, and 0.1% Tween20) and then incubated with anti-C1s (LS-C483829, LS Bio 1:500) or anti-GAPDH (Thermo Fisher Sci., MA515738, 1:5,000) primary antibodies overnight at 4°C. Membranes were incubated with an HRP-conjugated anti-rabbit (Cell Signaling, 7074) or HRP-linked anti-mouse (Cell Signaling, 7076) secondary antibody. Immunoreactive bands were detected using ECL LiteAbTol plus kit A + B (Euroclone, GEHRPN2235) with an Alliance LD2 device and software (UVITEC). C1s and GAPDH signal intensities were analyzed with ImageJ.

Cell isolation and culture

Single myofibers were isolated from the *extensor digitorum longus* mouse muscles as previously described (de Morrée et al, 2017). To obtain mononucleated cells, murine hindlimb, diaphragm muscles, or human biopsies were processed as previously described (Liu et al, 2015). Fluorescence-activated cell sorting (FACS) Aria III cell sorter (BD Biosciences) was used to separate cell populations. Mouse-derived MuSCs were purified by negative selection with anti-CD31, anti-CD45, and anti-Sca1 antibodies and positive selection with antivascular cell adhesion molecule (VCAM) antibody (Liu et al, 2015), mouse-derived FAPs were purified by negative selection with anti-CD31 and anti-CD45 antibodies and positive selection with an anti-Sca1 antibody (Judson et al, 2017), while human-derived FAPs were purified by negative selection with anti-CD31 and anti-CD45 antibodies and positive selection with an anti-CD34 antibody (Farup et al, 2021), and mouse-derived macrophages were purified by positive selection with anti-CD45 and anti-F4/80 antibodies. For specific experiments, mouse-derived macrophages were fractionated with an anti-CD206 antibody. CD45^{-ve}CD31^{-ve} cells are indicated as Lin^{-ve} cells, whereas CD45⁺CD31⁺ cells are indicated as Lin⁺ cells. A list of primary antibodies used is enclosed in Appendix Table S4. APC Streptavidin (1:100, BioLegend) was added to samples incubated with a biotin-conjugated anti-VCAM antibody. After sorting, cells were cultured and processed for immunostaining or RNA extraction. Mouse FAPs were cultured in DMEM supplemented with 10% fetal bovine serum (FBS) de-complemented by heat inactivation and 2.5 ng/ml basic fibroblast growth factor (bFGF, LSBio). For immunostaining, cells were resuspended in Ham's F-10 supplemented with 20% FBS and allowed to adhere overnight on glass ECM-coated slides (Merck).

C2C12, RAW-264.7, HEK-293, C3H-10T1/2, NIH-3T3, and STO were obtained from ATCC and maintained in DMEM supplemented with 10% FBS de-complemented by heat inactivation. C57 primary myoblasts were isolated from C57BL/6J mice as previously described (Rando & Blau, 1994; Biressi et al, 2014). Primary cultures were plated on 5 µg/ml laminin/collagen-coated dishes and amplified in Ham's F-10 with 20% FBS, and 2.5 ng/ml bFGF was added to the culture every 24 h. All cell lines were mycoplasma free. In the experiments with mice sera, C2C12 cells were cultured in DMEM supplemented with 5% mice serum collected from WT or MDX mice. In experiments with conditioned media, STO, and RAW-264.7, cells were allowed to reach confluence for 4.5 days. Media

were collected and filtered through a 0.42 µm filter. STO and RAW-264.7 media were combined in an 8:1 ratio, which was previously calculated from *in vivo* analysis of the proportion of macrophages and FAPs in MDX muscles (Appendix Table S5). Reagents used are as follows: XAV-939 (Merck, 100 µM), WNT3A (StemRD, 50–100 ng/ml), C1q (Sigma, 100 µg/ml), C1r (BIOPUR, 25 µg/ml), C1s (BIOPUR, 25 µg/ml), and C1r/s inhibitor (Merck, 100 µg/ml).

Quantitative RNA analysis

RNA was extracted using TRIzol Reagent (Invitrogen), and RNA was reverse transcribed using High-Capacity cDNA Reverse Transcription Kit (Thermo Fisher Scientific) according to the manufacturer's instructions. Gene expression was measured by quantitative RT-PCR using SYBR Green Master Mix (Thermo Fisher Scientific). The efficiency of all primers was calculated as $\geq 96\%$. Primers are indicated in Appendix Table S6. Relative quantification was normalized to mouse or human hypoxanthine-guanine phosphoribosyltransferase (HPRT). UMAP plots referred to the expression of C1 components, CD206, and IL-10 in human muscles were produced with Plotly.js (v2.11.0) and obtained from Tabula Sapiens single-cell transcriptomic analysis (Jones et al, 2022). The dataset referred to C1 and CD163 expression in mouse limbs is available in the following database: Tabula Muris Dataset: <https://tabula-muris.ds.czbiohub.org/> (Tabula Muris Consortium et al, 2018).

Human biopsies

The Biobank of skeletal muscle, peripheral nerve, DNA, and cell lines—IRCCS Ca' Granda Ospedale Maggiore Policlinico, Milan (request No 1504)—provided the human biopsies used for C1 expression. Muscle biopsies for FACS and immunofluorescence analysis were collected from orthopedic surgery. Procedures were performed under the International Conference on Harmonisation of Good Clinical Practice guidelines, the Declaration of Helsinki (2008), the Department of Health and Human Services Belmont Report, and the European Directive 2001/20/EC. Informed consent was obtained after the nature and possible consequences of the study were explained. A list of human biopsies used in this study is enclosed in Appendix Table S1.

Immunofluorescence, cross-sectional area analysis, interstitial fibrotic area calculation, and hematoxylin-eosin staining

Cells and muscle sections were processed for immunofluorescence as previously described (Biressi et al, 2013). Briefly, dissected muscles were fixed for 4 h using 0.5% paraformaldehyde, then transferred to 30% sucrose overnight, frozen in optimum cutting temperature compound (OCT), and cryosectioned at 8 µm. For morphometric and fibrotic area quantification, HSP47 and TGFβ2 quantification muscles were directly frozen in nitrogen-cooled isopentane and cryosectioned at 6 µm. The acquisition was made with a Zeiss Axio Observer Z1 optical microscope equipped with a monochrome camera (AxioCam 503 mono D), with Nikon AX confocal laser scanning microscope or Leica TCS SP8 confocal microscopy. Primary antibodies are listed in Appendix Table S7. Alexa Fluor 488/594/647 secondary antibodies (Thermo Fisher Scientific) were used.

Zen 2 software (Zeiss) and ImageJ were used for immunofluorescence analysis. Normal or non-normal dataset distribution, Spearman (r), and Pearson coefficient (r) were determined with GraphPad Prism software.

Details of the performed quantifications are the following: (i) C1q pixel intensity quantification in *WT* versus *MDX gastrocnemius* (Fig 1K): For each biological replicate, 9–44 different regions of the muscle were evaluated for C1q staining, and 5–18 different regions were evaluated for background signal (staining with only secondary antibody). The average background value was subtracted from the average C1q pixel intensity value for each biological replicate. Pixel intensity was calculated using ZEN 2 software (Zeiss). (ii) Axin2 pixel intensity quantification in human sections (Appendix Fig S1B): For each biological replicate, 8–59 different regions within the regenerating/interstitial muscle portions were evaluated for Axin2 staining, and 9–34 different regions were evaluated for background (staining with only secondary antibody). The background staining was used to evaluate the specificity of Axin2 staining. Pixel intensity was calculated using ZEN 2 software (Zeiss). (iii) TGF β 2 pixel intensity quantification in human sections (Appendix Fig S1C): For each biological replicate, 11–22 different regions (images) of the regenerating/interstitial muscle areas were evaluated for TGF β 2 staining, and 8 to 15 different regions (images) were evaluated for background (staining with only secondary antibody). The average background intensity value was subtracted from the corresponding TGF β 2 signal for each biological sample. Pixel intensity values were calculated with ImageJ. (iv) C1s pixel intensity quantification in *WT* versus *MDX gastrocnemius* (Appendix Fig S3A): For each biological replicate, 8–28 different regions of the muscle were evaluated for C1s staining, and 4–18 different regions were evaluated for background signal (staining with only secondary antibody). For each biological replicate, the average background value was subtracted from the average C1s pixel intensity value. Pixel intensity was calculated using ZEN 2 software (Zeiss). (v) Axin2 and TGF β 2 pixel intensity quantification in *WT* and *MDX* PDGFR α^{+ve} cells (Fig EV1A and B): Axin2 pixel intensity was measured in 131 (for *WT*) and 130 (for *MDX*) PDGFR α^{+ve} cells. TGF β 2 pixel intensity was measured in 126 (for *WT*) and 215 (for *MDX*) PDGFR α^{+ve} cells. The average background intensity was calculated by averaging the intensity of cells stained only with secondary antibodies (46 cells for *WT* and 48 cells for *MDX*) and was subtracted from each measurement. For each biological sample, 7–25 different regions were analyzed for Axin2, 10 to 28 different regions were analyzed for TGF β 2, and 3–4 different regions were analyzed for background intensities. Pixel intensity was calculated using ZEN 2 software (Zeiss). (vi) C1q and C1s pixel intensity quantification in FACS-isolated cells from human muscles (Appendix Fig S6G and H): The maximum pixel intensity was measured in cells stained with anti-C1q and anti-C1s antibodies. C1s was evaluated in 478 FAPs, 171 CD45 $^{+ve}$ cells, and 206 CD31 $^{+ve}$ pooled from four (FAPs and CD31 $^{+ve}$ cells) and three (CD45 $^{+ve}$ cells) independent experiments. C1q signal was evaluated in 109 FAPs, and 187 CD45 $^{+ve}$ pooled from three (FAPs) and two (CD45 $^{+ve}$ cells) independent experiments. The background signal was evaluated in each biological sample using the staining with only secondary antibodies. Specific signal intensities and the extreme top and bottom 5% of the population were excluded. Pixel intensity was calculated using ZEN 2 software (Zeiss). (vii) Macrophages and FAPs distance analysis (Fig 4A and C): The distance between

macrophages and FAPs was analyzed by measuring the distance of each macrophage from its closest FAP (nucleus to nucleus); for each biological replicate, 60–200 macrophages were selected in at least 20 different muscle areas; Appendix Fig S11C and D: The distance between FAPs and macrophages was analyzed by measuring the distance of each FAP from its closest macrophage (nucleus to nucleus); for each biological replicate, 100–350 FAPs were selected in at least four different muscles' areas; Fig EV4B and D: The distance between macrophages and FAPs was analyzed by measuring the distance of each macrophage from its closest FAP (nucleus to nucleus); for each biological replicate, 261–307 macrophages were selected in 17–44 (*WT* INJ), 11–34 (*MDX*), and 8–13 (fib-*MDX*) different muscles' areas. (viii) C1q/Axin2 and C1q/TGF β 2 correlation analysis in *MDX* muscles (Fig 4D and E): The average pixel intensity of C1q, Axin2, and TGF β 2 was measured for each biological replicate in 45–94 randomly selected regions of 1,029 μm^2 within the regenerating areas of the muscle. The background pixel intensity measured on sections stained only with the secondary antibody was subtracted. Images were acquired with a Leica TCS SP8 confocal microscope. Pixel intensity was calculated using ImageJ. (ix) TGF β 2 $^{+ve}$ FAPs quantification in *MDX* and fib-*MDX* muscles (Fig EV4I): The percentage of TGF β 2 $^{+ve}$ cells was calculated on a total number of 1,162 (*MDX*) and 1,319 (fib-*MDX*) PDGFR α^{+ve} cells. For each biological sample, 3–10 different randomly selected muscle regions were analyzed. (x) Myofiber cross-sectional area (CSA) analysis: The myofiber cross-sectional area (CSA) was measured in 201–372 (Fig 6I) and 351–415 (Fig EV5N) randomly selected fibers for each biological replicate, and the median values of these measurements were calculated. (xi) Collagen 1 and collagen 3 pixel intensity in muscles (Fig 6J and Appendix Fig S15I): The average collagens 1 and 3 pixel intensity was calculated for each biological replicate in 17 to 27 randomly selected interstitial regions within the muscle sections. For each biological sample, the average background value was calculated from at least nine different randomly selected regions of the muscle stained with only the secondary antibody. The corresponding average background value was subtracted from each collagen 1 and collagen 3 signal intensity measurement. Pixel intensity was calculated using ZEN 2 software (Zeiss); (Fig EV5O): The average collagen 1 pixel intensity was calculated for each biological replicate in 31–45 randomly selected interstitial regions within the muscle sections. For each biological replicate, the average background staining was evaluated in 10–16 randomly selected muscle areas stained with only the secondary antibody. The corresponding average background value was subtracted from each collagen 1 signal intensity measurement. Pixel intensity was calculated using ImageJ. (xii) TGF β 2 pixel intensity quantification in CNTR and C1r/s INH muscles: TGF β 2 average pixel intensity was measured in 155 (CNTR) and 320 (C1r/s INH) PDGFR α^{+ve} cells. For each biological sample, TGF β 2 $^{+ve}$ cells were analyzed in 7–14 different muscle regions. For each biological sample, the average background value was calculated from at least 30 cells stained with only secondary antibodies, and randomly selected in at least three different muscle regions. The corresponding average background value was subtracted from each TGF β 2 signal intensity measurement. Pixel intensity was calculated using ZEN 2 software (Zeiss). (xiii) HSP47 pixel intensity quantification in CNTR and C1r/s INH PDGFR α^{+ve} cells (Appendix Fig S15B): HSP47 average pixel intensity was measured in 209 (CNTR) and 234 (C1r/s INH) PDGFR α^{+ve}

The paper explained

Problem

Fibrosis is associated with compromised muscle functionality in Duchenne muscular dystrophy. It contributes to the symptomatology of the disease and is a barrier to effective therapies. Elevated WNT signaling has been shown to play a detrimental role in muscle regeneration and promote the accumulation of fibrosis in dystrophic muscles. However, the molecular and cellular pathways responsible for this process are poorly characterized.

Results

We found increased levels of complement C1 in the skeletal muscles of both dystrophic patients and mice compared to healthy controls. We report here observations supporting the existence of a crosstalk between the complement and the WNT signaling pathways. Macrophages and fibro-adipogenic progenitors are increased in the *MDX* muscles proximal to the *bona fide* regenerating areas and secrete distinct subunits of the C1 complex (i.e., C1q and C1r/s, respectively). Similar results were obtained in human muscles. The enhanced complement levels positively correlated with the increased expression of WNT-target proteins in the *MDX*-regenerating areas. Furthermore, C1 complex induced WNT signaling in murine FACS-isolated fibro-adipogenic progenitors, fibroblasts, and myoblasts *in vitro*. The *in vivo* pharmacological inhibition of C1r/s in the accelerated fib-*MDX* murine model of muscular dystrophy led to the amelioration of the dystrophic phenotype (i.e., reduced expression of WNT signaling targets and fibrogenic genes in the dystrophic fibro-adipogenic progenitor cells, and reduced collagen deposition in the muscle interstitium).

Impact

Our data support that complement is detrimental in the dystrophic environment and that inhibiting the classical complement pathway can reduce consequential tissue destruction. Our data provide evidence linking complement with degenerative disease and support the investigation of novel therapeutic strategies to delay the progression of Duchenne muscular dystrophy.

cells For each biological sample, PDGFR α ⁺ cells were analyzed in 4–12 different muscle regions. For each biological sample, the average background value was calculated from at least 30 cells stained with only secondary antibodies and randomly selected in at least three different muscle regions. The corresponding average background value was subtracted from each HSP47 signal intensity measurement. Pixel intensity was calculated using ZEN 2 software (Zeiss).

The interstitial fibrotic area was calculated as the percentage of the area with collagen 1 deposition over the total muscle area: Fig 6H: For each biological replicate, 510–904 (CNTR) and 144–497 (C1r/s INH) areas were evaluated for collagen deposition in 11–13 (CNTR) and 10–20 (C1r/s INH) different randomly selected muscles regions and the average fibrotic area value was calculated; Fig EV5M: For each biological replicate, 187–342 (CNTR) and 62–312 (C1r/s INH) areas were evaluated for collagen deposition in 4–5 (CNTR) and 4–7 (C1r/s INH) different randomly selected muscle regions, and the average fibrotic area value was calculated.

For hematoxylin/eosin (H&E) staining, muscles were flash-frozen in isopentane, and mid-belly cryostat sections (8 μ m) were processed as previously described (George *et al.*, 2013).

Study design and statistical analysis

A primary objective of this study was to evaluate the levels and the role of complement C1 in the skeletal muscles during the dystrophic progression. For this purpose, we compared *MDX* mice with age-matched *WT* controls and DMD human biopsies with healthy controls, and we analyzed fib-*MDX* mice after inhibiting the complement pathway. We aimed to investigate the C1/WNT axis in murine muscle cells and dystrophic tissues and to evaluate the C1/WNT axis as a regulator of the FAPs' behavior. Preliminary data and similar studies previously performed with cells and tissues collected from aging and dystrophic mice indicated that 3–10 biological replicates were required in each group to detect a 20% difference in the amounts of gene expression and morphometric measures with a power of 0.8 and significance level of 0.05. Experiments were not blinded. Animals were randomly assigned to experimental and treatment groups based on availability and genotype.

Unless otherwise stated, data are presented as mean \pm SEM, one-way ANOVA test was performed for multiple comparisons, and parametric or non-parametric Student's *t*-tests were performed for comparison between two groups. Statistical analysis was performed using GraphPad Prism. The number of biological replicates and tests used to calculate statistical differences are reported in each figure legend. Significant *P*-values are reported in graphs or tables.

Data availability

This study includes no data deposited in external repositories.

Expanded View for this article is available [online](#).

Acknowledgements

We thank Bert Blaauw, Ted Yednock, Rick Artis, and Luciano Conti for their helpful discussions. We acknowledge CSL Behring for kindly providing us with the C1r/s inhibitor Berinert. We thank Alessandro Alaimo, Silvia Accordini, Vaibhav Gharat, and Sofia Gaspari for their technical help and suggestions. We are grateful to Maurizio Moggio, director of the Biobank at IRCCS Fondazione Ca' Granda Ospedale Maggiore Policlinico, for providing us with human specimens. The Biobank of skeletal muscle, peripheral nerve, DNA, and cell lines is a member of the Telethon Network of Genetic Biobanks (project No. GTB12001), funded by Telethon Italy, and of the EuroBioBank network. CIBIO Core Facilities are supported by the European Regional Development Fund (ERDF) 2014–2020. Work in the authors' laboratory is supported by the Muscular Dystrophy Association—United States (innovation grant No. 874294 to SB), Association Française contre les Myopathies (AFM)—France (grant No. 23758 to SB), Fondazione Telethon and Provincia autonoma di Trento—Italy (grant No. TCP13007 to SB), POR FESR Regione Lombardia 16 (FORCE-4-CURE, grant No. 2526393 to YT), Ministero della Salute (grant No. RF-2016-02362263 to YT), and GFB-ONLUS (grant No. PR-0394 to YT).

Author contributions

Stefano Biressi: Conceptualization; data curation; formal analysis; supervision; funding acquisition; investigation; visualization; methodology; writing – original draft; project administration; writing – review and editing. **Francesca Florio:** Conceptualization; data curation; formal analysis; investigation; visualization; methodology; writing – original draft; project administration; writing – review and editing. **Sara Vencato:** Investigation;

methodology. **Filomena T Papa:** Formal analysis; methodology.

Michela Libergoli: Methodology. **Eyemen Kheir:** Methodology.

Imen Ghzaïel: Methodology. **Thomas A Rando:** Conceptualization.

Yvan Torrente: Resources; funding acquisition; writing – original draft; writing – review and editing.

Disclosure and competing interests statement

FF and SB compare as inventors in U.S. Provisional Patent Application No. 63/270352 and subsequent PCT Application No. PCT/US22/78510 filed by relevant institutions based on part of the results described in this manuscript. All other authors declare that they have no conflict of interest.

For more information

For more information about the topics presented in this paper please visit the following websites: (i) <https://www.cibio.unitn.it/220/dulbecco-telethon-laboratory-of-stem-cells-and-regenerative-medicine> (Laboratory of Stem Cell and Regenerative Medicine website). (ii) DMD OMIM: <https://www.omim.org/entry/310200>.

References

- Akhmetshina A, Palumbo K, Dees C, Bergmann C, Venalis P, Zerr P, Horn A, Kireva T, Beyer C, Zwerina J *et al* (2012) Activation of canonical Wnt signalling is required for TGF- β -mediated fibrosis. *Nat Commun* 3: 735
- Babaeijandaghi F, Cheng R, Kajabadi N, Soliman H, Chang CK, Smandych J, Tung LW, Long R, Ghassemi A, Rossi FMV (2022) Metabolic reprogramming of skeletal muscle by resident macrophages points to CSF1R inhibitors as muscular dystrophy therapeutics. *Sci Transl Med* 14: eabg7504
- Biressi S, Bjornson CRR, Carlign PMM, Nishijo K, Keller C, Rando TA (2013) Myf5 expression during fetal myogenesis defines the developmental progenitors of adult satellite cells. *Dev Biol* 379: 195–207
- Biressi S, Miyabara EH, Gopinath SD, Carlign PMM, Rando TA (2014) A Wnt-TGF β 2 axis induces a fibrogenic program in muscle stem cells from dystrophic mice. *Sci Transl Med* 6: 267ra176
- Biressi S, Filareto A, Rando TA (2020) Stem cell therapy for muscular dystrophies. *J Clin Invest* 130: 5652–5664
- Birnkrant DJ, Bushby K, Bann CM, Apkon SD, Blackwell A, Brumbaugh D, Case LE, Clemens PR, Hadjiyannakis S, Pandya S *et al* (2018) Diagnosis and management of Duchenne muscular dystrophy, part 1: diagnosis, and neuromuscular, rehabilitation, endocrine, and gastrointestinal and nutritional management. *Lancet Neurol* 17: 251–267
- Blyszczuk P, Müller-Edenborn B, Valenta T, Osto E, Stellato M, Behnke S, Glatz K, Basler K, Lüscher TF, Distler O *et al* (2017) Transforming growth factor- β -dependent Wnt secretion controls myofibroblast formation and myocardial fibrosis progression in experimental autoimmune myocarditis. *Eur Heart J* 38: 1413–1425
- Brack AS, Conboy MJ, Roy S, Lee M, Kuo CJ, Keller C, Rando TA (2007) Increased Wnt signaling during aging alters muscle stem cell fate and increases fibrosis. *Science* 317: 807–810
- Burzyn D, Kuswanto W, Kolodin D, Shadrach JL, Cerletti M, Jang Y, Sefik E, Tan TG, Wagers AJ, Benoist C *et al* (2013) A special population of regulatory T cells potentiates muscle repair. *Cell* 155: 1282–1295
- Carthy JM, Garmaroudi FS, Luo Z, McManus BM (2011) Wnt3a induces myofibroblast differentiation by upregulating TGF- β signaling through SMAD2 in a β -Catenin-dependent manner. *PLoS ONE* 6: e19809
- Chen HZ, Tsai SY, Leone G (2009) Emerging roles of E2Fs in cancer: an exit from cell cycle control. *Nat Rev Cancer* 9: 785–797
- Ciciliot S, Schiaffino S (2010) Regeneration of mammalian skeletal muscle. Basic mechanisms and clinical implications. *Curr Pharm Des* 16: 906–914
- Cisternas P, Vio CP, Inestrosa NC (2014) Role of Wnt signaling in tissue fibrosis, lessons from skeletal muscle and kidney. *Curr Mol Med* 14: 510–522
- Contreras O, Rebolledo DL, Oyarzún JE, Olgúin HC, Brandan E (2016) Connective tissue cells expressing fibro/adipogenic progenitor markers increase under chronic damage: relevance in fibroblast-myofibroblast differentiation and skeletal muscle fibrosis. *Cell Tissue Res* 364: 647–660
- de Morrée A, van Velthoven CTJ, Gan Q, Salvi JS, Klein JDD, Akimenko I, Quarta M, Biressi S, Rando TA (2017) Staufen1 inhibits MyoD translation to actively maintain muscle stem cell quiescence. *Proc Natl Acad Sci USA* 114: E8996–E9005
- Desguerre I, Mayer M, Leturcq F, Barbet J-P, Gherardi RK, Christov C (2009) Endomysial fibrosis in Duchenne muscular dystrophy: a marker of poor outcome associated with macrophage alternative activation. *J Neuropathol Exp Neurol* 68: 762–773
- Desguerre I, Arnold L, Vignaud A, Cuvelier S, Yacoub-Youssef H, Gherardi RK, Chelly J, Chretien F, Mounier R, Ferry A *et al* (2012) A new model of experimental fibrosis in hindlimb skeletal muscle of adult mdx mouse mimicking muscular dystrophy. *Muscle Nerve* 45: 803–814
- Dulauroy S, Di Carlo SE, Langa F, Eberl G, Peduto L (2012) Lineage tracing and genetic ablation of ADAM12(+) perivascular cells identify a major source of profibrotic cells during acute tissue injury. *Nat Med* 18: 1262–1270
- Emery AEH (2002) The muscular dystrophies. *Lancet* 359: 687–695
- Engel AG, Biesecker G (1982) Complement activation in muscle fiber necrosis: demonstration of the membrane attack complex of complement in necrotic fibers. *Ann Neurol* 12: 289–296
- Epelman S, Liu PP, Mann DL (2015) Role of innate and adaptive immune mechanisms in cardiac injury and repair. *Nat Rev Immunol* 15: 117–129
- Farup J, Just J, de Paoli F, Lin L, Jensen JB, Billeskov T, Roman IS, Cömert C, Møller AB, Madaro L *et al* (2021) Human skeletal muscle CD90 + fibro-adipogenic progenitors are associated with muscle degeneration in type 2 diabetic patients. *Cell Metab* 33: 2201–2214
- Feussner A, Kalina U, Hofmann P, Machnig T, Henkel G (2014) Biochemical comparison of four commercially available C1 esterase inhibitor concentrates for treatment of hereditary angioedema. *Transfusion* 54: 2566–2573
- Finsterer J, Stöllberger C (2003) The heart in human dystrophinopathies. *Cardiology* 99: 1–19
- Florio F, Accordini S, Libergoli M, Biressi S (2022) Targeting muscle-resident single cells through in vivo electro-enhanced plasmid transfer in healthy and compromised skeletal muscle. *Front Physiol* 13: 834705
- Foidart M, Foidart JM, Engel WK (1981) Collagen localization in normal and fibrotic human skeletal muscle. *Arch Neurol* 38: 152–157
- George RM, Biressi S, Beres BJ, Rogers E, Mulia AK, Allen RE, Rawls A, Rando TA, Wilson-Rawls J (2013) Numb-deficient satellite cells have regeneration and proliferation defects. *Proc Natl Acad Sci USA* 110: 18549–18554
- Girardi F, Le Grand F (2018) Wnt signaling in skeletal muscle development and regeneration. *Prog Mol Biol Transl Sci* 153: 157–179
- Gulati P, Lemerrier C, Lappin D, Whaley K, Gue D (1994) Expression of the components and regulatory proteins of the classical pathway of complement in normal and diseased synovium. *Rheumatol Int* 14: 13–19
- Heredia JE, Mukundan L, Chen FM, Mueller AA, Deo RC, Locksley RM, Rando TA, Chawla A (2013) Type 2 innate signals stimulate fibro/adipogenic progenitors to facilitate muscle regeneration. *Cell* 153: 376–388

- Ieronimakis N, Hays A, Prasad A, Janebodini K, Duffield JS, Reyes M (2016) PDGFR α signalling promotes fibrogenic responses in collagen-producing cells in Duchenne muscular dystrophy. *J Pathol* 240: 410–424
- Jäger U, D'Sa S, Schörghofer C, Bartko J, Derhaschnig U, Sillaber C, Jilka-Stohlawetz P, Fillitz M, Schenk T, Patou G et al (2019) Inhibition of complement C1s improves severe hemolytic anemia in cold agglutinin disease: a first-in-human trial. *Blood* 133: 893–901
- Joe AWB, Yi L, Natarajan A, Le Grand F, So L, Wang J, Rudnicki MA, Rossi FMV (2010) Muscle injury activates resident fibro/adipogenic progenitors that facilitate myogenesis. *Nat Cell Biol* 12: 153–163
- Jones RC, Karkanas J, Krasnow MA, Pisco AO, Quake SR, Salzman J, Yosef N, Bulthaupt B, Brown P, Harper W et al (2022) The Tabula Sapiens: a multiple-organ, single-cell transcriptomic atlas of humans. *Science* 376: eabl4896
- Judson RN, Low M, Eisner C, Rossi FM (2017) Isolation, culture, and differentiation of Fibro/Adipogenic Progenitors (FAPs) from skeletal muscle. *Methods Mol Biol* 1668: 93–103
- Kusumoto H, Hirose S, Salier JP, Hagen FS, Kurachi K (1988) Human genes for complement components C1r and C1s in a close tail-to-tail arrangement. *Proc Natl Acad Sci USA* 85: 7307–7311
- Lemos DR, Babaeijandaghi F, Low M, Chang C-K, Lee ST, Fiore D, Zhang R-H, Natarajan A, Nedospasov SA, Rossi FMV (2015) Nilotinib reduces muscle fibrosis in chronic muscle injury by promoting TNF-mediated apoptosis of fibro/adipogenic progenitors. *Nat Med* 21: 786–794
- Liu L, Cheung TH, Charville GW, Rando TA (2015) Isolation of skeletal muscle stem cells by fluorescence-activated cell sorting. *Nat Protoc* 10: 1612–1624
- Liu F, Liang Z, Xu J, Li W, Zhao D, Zhao Y, Yan C (2016) Activation of the wnt/ β -catenin signaling pathway in polymyositis, dermatomyositis and Duchenne muscular dystrophy. *J Clin Neurol* 12: 351–360
- Liu X, Liu Y, Zhao L, Zeng Z, Xiao W, Chen P (2017) Macrophage depletion impairs skeletal muscle regeneration: the roles of regulatory factors for muscle regeneration. *Cell Biol Int* 41: 228–238
- McDonald CM, Henricson EK, Abresch RT, Duong T, Joyce NC, Hu F, Clemens PR, Hoffman EP, Cnaan A, Gordish-Dressman H et al (2018) Long-term effects of glucocorticoids on function, quality of life, and survival in patients with Duchenne muscular dystrophy: a prospective cohort study. *Lancet* 391: 451–461
- McGreevy JW, Hakim CH, McIntosh MA, Duan D (2015) Animal models of Duchenne muscular dystrophy: from basic mechanisms to gene therapy. *Dis Model Mech* 8: 195–213
- Mercuri E, Bönnemann CG, Muntoni F (2019) Muscular dystrophies. *Lancet* 394: 2025–2038
- Molina T, Fabre P, Dumont NA (2021) Fibro-adipogenic progenitors in skeletal muscle homeostasis, regeneration and diseases. *Open Biol* 11: 210110
- Mozzetta C, Consalvi S, Saccone V, Tierney M, Diamantini A, Mitchell KJ, Marazzi G, Borsellino G, Battistini L, Sassoon D et al (2013) Fibroadipogenic progenitors mediate the ability of HDAC inhibitors to promote regeneration in dystrophic muscles of young, but not old Mdx mice. *EMBO Mol Med* 5: 626–639
- Mueller AA, van Velthoven CT, Fukumoto KD, Cheung TH, Rando TA (2016) Intronic polyadenylation of PDGFR α in resident stem cells attenuates muscle fibrosis. *Nature* 540: 276–279
- Nagao N, Shomura I, Sawada Y (1987) Serum activity of C1 inactivator in Duchenne-type progressive muscular dystrophy. *Biochem Med Metab Biol* 37: 385–388
- Naito AT, Sumida T, Nomura S, Liu M-LL, Higo T, Nakagawa A, Okada K, Sakai T, Hashimoto A, Hara Y et al (2012) Complement C1q activates canonical Wnt signaling and promotes aging-related phenotypes. *Cell* 149: 1298–1313
- O'Brien KF, Kunkel LM (2001) Dystrophin and muscular dystrophy: past, present, and future. *Mol Genet Metab* 74: 75–88
- Pessina P, Kharraz Y, Jardí M, Fukada S, Serrano AL, Perdiguer E, Muñoz-Cánoves P (2015) Fibrogenic cell plasticity blunts tissue regeneration and aggravates muscular dystrophy. *Stem Cell Reports* 4: 1046–1060
- Porter JD, Khanna S, Kaminski HJ, Rao JS, Merriam AP, Richmonds CR, Leahy P, Li J, Guo W, Andrade FH (2002) A chronic inflammatory response dominates the skeletal muscle molecular signature in dystrophin-deficient mdx mice. *Hum Mol Genet* 11: 263–272
- Purcu DU, Korkmaz A, Gunalp S, Helvacı DG, Erdal Y, Dogan Y, Suner A, Wingender G, Sag D (2022) Effect of stimulation time on the expression of human macrophage polarization markers. *PLoS ONE* 17: e0265196
- Rando TA, Blau HM (1994) Primary mouse myoblast purification, characterization, and transplantation for cell-mediated gene therapy. *J Cell Biol* 125: 1275–1287
- Reis ES, Mastellos DC, Yancopoulos D, Risitano AM, Ricklin D, Lambris JD (2015) Applying complement therapeutics to rare diseases. *Clin Immunol* 161: 225–240
- Scharner J, Zammit PS (2011) The muscle satellite cell at 50: the formative years. *Skelet Muscle* 1: 28
- Sellar GC, Blake DJ, Reid KBM (1991) Characterization and organization of the genes encoding the A-, B- and C-chains of human complement subcomponent C1q. The complete derived amino acid sequence of human C1q. *Biochem J* 274: 481–490
- Seo HH, Lee S, Lee CY, Lee J, Shin S, Song BW, Kim IK, Choi JW, Lim S, Kim SW et al (2018) Multipoint targeting of TGF- β /Wnt transactivation circuit with microRNA 384-5p for cardiac fibrosis. *Cell Death Differ* 26: 1107–1123
- Serrano AL, Muñoz-Cánoves P (2010) Regulation and dysregulation of fibrosis in skeletal muscle. *Exp Cell Res* 316: 3050–3058
- Sewry CA, Dubowitz V, Abrahams A, Luzzio JP, Campbell AK (1987) Immunocytochemical localisation of complement components C8 and C9 in human diseased muscle. The role of complement in muscle fibre damage. *J Neurol Sci* 81: 141–153
- Shen W, Li Y, Zhu J, Schwendener R, Huard J (2008) Interaction between macrophages, TGF- β 1, and the COX-2 pathway during the inflammatory phase of skeletal muscle healing after injury. *J Cell Physiol* 214: 405–412
- Sousa-Victor P, García-Prat L, Muñoz-Cánoves P (2022) Control of satellite cell function in muscle regeneration and its disruption in ageing. *Nat Rev Mol Cell Biol* 23: 204–226
- Spuler S, Engel AG (1998) Unexpected sarcolemmal complement membrane attack complex deposits on nonnecrotic muscle fibers in muscular dystrophies. *Neurology* 50: 41–46
- Sumida T, Naito AT, Nomura S, Nakagawa A, Higo T, Hashimoto A, Okada K, Sakai T, Ito M, Yamaguchi T et al (2015) Complement C1q-induced activation of β -catenin signalling causes hypertensive arterial remodelling. *Nat Commun* 6: 6241
- Tabula Muris Consortium, Overall coordination, Logistical coordination, Organ collection and processing, Library preparation and sequencing, Computational data analysis, Cell type annotation, Writing group, Supplemental text writing group & Principal investigators (2018) Single-cell transcriptomics of 20 mouse organs creates a Tabula Muris. *Nature* 562: 367–372
- Tao H, Yang J-J, Shi K-H, Li J (2016) Wnt signaling pathway in cardiac fibrosis: new insights and directions. *Metabolism* 65: 30–40

- Tidball JG, Villalta SA (2010) Regulatory interactions between muscle and the immune system during muscle regeneration. *Am J Physiol Regul Integr Comp Physiol* 298: R1173–R1187
- Trenz F, Haroun S, Cloutier A, Richter MV, Grenier G (2010) A muscle resident cell population promotes fibrosis in hindlimb skeletal muscles of mdx mice through the Wnt canonical pathway. *Am J Physiol Cell Physiol* 299: C939–C947
- Tripodi L, Villa C, Molinaro D, Torrente Y, Farini A (2021) The immune system in Duchenne muscular dystrophy pathogenesis. *Biomedicine* 9: 1447
- Uezumi A, Fukada S, Yamamoto N, Takeda S, Tsuchida K (2010) Mesenchymal progenitors distinct from satellite cells contribute to ectopic fat cell formation in skeletal muscle. *Nat Cell Biol* 12: 143–152
- Uezumi A, Ito T, Morikawa D, Shimizu N, Yoneda T, Segawa M, Yamaguchi M, Ogawa R, Matev MM, Miyagoe-Suzuki Y et al (2011) Fibrosis and adipogenesis originate from a common mesenchymal progenitor in skeletal muscle. *J Cell Sci* 124: 3654–3664
- Villalta SA, Nguyen HX, Deng B, Gotoh T, Tidball JG (2009) Shifts in macrophage phenotypes and macrophage competition for arginine metabolism affect the severity of muscle pathology in muscular dystrophy. *Hum Mol Genet* 18: 482–496
- Wang X, Zhou L (2022) The many roles of macrophages in skeletal muscle injury and repair. *Front Cell Dev Biol* 10: 952249
- Wang X, Zhao W, Ransohoff RM, Zhou L (2016) Identification and function of fibrocytes in skeletal muscle injury repair and muscular dystrophy. *J Immunol* 197: 4750–4761
- Wang X, Sathe AA, Smith GR, Ruf-Zamojski F, Nair V, Lavine KJ, Xing C, Sealton SC, Zhou L (2020) Heterogeneous origins and functions of mouse skeletal muscle-resident macrophages. *Proc Natl Acad Sci USA* 117: 20729–20740
- Wosczyzna MN, Rando TA (2018) A muscle stem cell support group: coordinated cellular responses in muscle regeneration. *Dev Cell* 46: 135–143
- Wosczyzna MN, Konishi CT, Perez Carbajal EE, Wang TT, Walsh RA, Gan Q, Wagner MW, Rando TA (2019) Mesenchymal stromal cells are required for regeneration and homeostatic maintenance of skeletal muscle. *Cell Rep* 27: 2029–2035



License: This is an open access article under the terms of the [Creative Commons Attribution](https://creativecommons.org/licenses/by/4.0/) License, which permits use, distribution and reproduction in any medium, provided the original work is properly cited.